

Attachment 1

MFN 08-878

“Finite Element Method for Acoustics”

Finite Element Modeling for Acoustics

W. Desmet, D. Vandepitte

The following document is a reformatted edition of the following reference:

W. Desmet, D. Vandepitte, 'Finite Element Method in Acoustics' in ISAAC13- International Seminar on Applied Acoustics, Leuven, 2002, ISBN 90-73802-73-3

© LMS International 2005



Chapter Two**2. Finite Element Modeling for Acoustics****W. Desmet^{*}, D. Vandepitte[†]****2.1 Introduction**

The finite element method is the most commonly used numerical prediction technique for solving engineering problems, which consist of finding the distribution of one (or several) field variable(s) in a continuum domain, governed by an appropriate (set of) partial differential equation(s) and boundary conditions.

The finite element method (see e.g. [2.52], [2.8] and [2.35]) is based on two concepts:

- * transformation of the original problem into an equivalent integral formulation (weighted residual or variational),
- * approximation of the field variable distributions and the geometry of the continuum domain in terms of a set of shape functions, which are locally defined within small subdomains ('finite elements') of the continuum domain.

Through the application of the element concept, the original problem of determining field variable distributions in a continuum domain is approximately transformed into a problem of determining the field variables at some discrete (nodal) positions within each element. This transformation results in a set of

* Professor at Katholieke Universiteit Leuven, Leuven, Belgium

† Full Professor at Katholieke Universiteit Leuven, Leuven, Belgium

algebraic equations, for which numerical solution procedures are readily available.

The use of the finite element method for acoustics was initiated by [2.30] and it has been applied in a concerted manner from the seventies onwards (see e.g., [2.20], [2.21], [2.44], [2.40]).

This chapter describes the use of the finite element method for solving time-harmonic acoustic problems. Based on the mathematical definition of an interior acoustic problem (section 2), the basic principles of the finite element method are discussed in section 3. In order to ensure the convergence of an acoustic finite element model, the proposed solution approximation must meet some necessary and sufficient convergence conditions, as outlined in section 4. The next section discusses the main properties of an (acoustic) finite element model. Section 6 addresses the direct and the modal approach for solving acoustic finite element models. Sections 7 and 8 discuss the extension of the finite element method for solving exterior acoustic problems and coupled vibro-acoustic problems. In the last section, several properties are illustrated through a simple, one-dimensional example.

2.2 Problem definition

The steady-state acoustic pressure p at any location (x, y, z) in a bounded fluid domain V , enclosed by a boundary surface Ω , due to a time-harmonic external source distribution q at frequency $\omega = 2\pi f$, is governed by the second-order Helmholtz equation

$$\nabla^2 p(x, y, z) + k^2 p(x, y, z) = -j\rho_0\omega q(x, y, z) \quad (2.1)$$

where $k = \omega/c = 2\pi f/c$ is the acoustic wavenumber, c is the speed of sound and ρ_0 is the ambient fluid mass density.

In order to uniquely define the pressure field in domain V , one boundary condition must be specified at each position on the closed boundary surface $\Omega = \Omega_p \cup \Omega_v \cup \Omega_z$:

- imposed pressure :

$$p = \bar{p} \quad \text{on } \Omega_p \quad (2.2)$$

- imposed normal velocity :

$$v_n = \frac{j}{\rho_0\omega} \frac{\partial p}{\partial n} = \bar{v}_n \quad \text{on } \Omega_v \quad (2.3)$$

- imposed normal impedance :

$$p = \bar{Z} v_n = \frac{v_n}{A} = \frac{j\bar{Z}}{\rho_0\omega} \frac{\partial p}{\partial n} = \frac{j}{\rho_0\omega A} \frac{\partial p}{\partial n} \quad \text{on } \Omega_z \quad (2.4)$$

2.3 Basic principles

The use of the finite element method for solving the above-defined interior acoustic problem, is based on the transformation of the problem into an equivalent weighted residual formulation (section 2.3.1). An approximation is introduced by expressing the pressure field in terms of a set of prescribed shape functions, which are locally defined within small subdomains ('finite elements') of the bounded fluid domain (section 2.3.2). In this way, the original problem of determining the pressure field at any position in the fluid domain may be approximately transformed into a problem of determining the pressure at some discrete positions in the fluid domain. This transformation results in a set of algebraic equations ('finite element model') (section 2.3.3).

2.3.1 Weighted residual formulation of the Helmholtz equation

The weighted residual concept provides an equivalent integral formulation of the Helmholtz Eq. (2.1). The concept defines a steady-state acoustic pressure field in a bounded fluid domain V as a pressure field, for which the integral equation

$$\int_V \tilde{p}(\nabla^2 p + k^2 p + j\rho_0 \omega q). dV = 0 \quad (2.5)$$

is satisfied for any weighting function \tilde{p} , that is bounded and uniquely defined within volume V and on its boundary surface Ω .

The weighted residual formulation (2.5) may be reformulated as

$$\begin{aligned} \int_V \left[\frac{\partial}{\partial x} (\tilde{p} \frac{\partial p}{\partial x}) + \frac{\partial}{\partial y} (\tilde{p} \frac{\partial p}{\partial y}) + \frac{\partial}{\partial z} (\tilde{p} \frac{\partial p}{\partial z}) \right]. dV - \int_V \left(\frac{\partial \tilde{p}}{\partial x} \frac{\partial p}{\partial x} + \frac{\partial \tilde{p}}{\partial y} \frac{\partial p}{\partial y} + \frac{\partial \tilde{p}}{\partial z} \frac{\partial p}{\partial z} \right). dV \\ + \int_V k^2 \tilde{p} p. dV + \int_V j\rho_0 \omega \tilde{p} q. dV = 0 \end{aligned} \quad (2.6)$$

or

$$\begin{aligned} \int_V (\nabla \tilde{p} \cdot \nabla p). dV - \omega^2 \int_V \left(\frac{1}{c^2} \tilde{p} p \right). dV = \\ \int_V j\rho_0 \omega \tilde{p} q. dV + \int_V \left[\frac{\partial}{\partial x} (\tilde{p} \frac{\partial p}{\partial x}) + \frac{\partial}{\partial y} (\tilde{p} \frac{\partial p}{\partial y}) + \frac{\partial}{\partial z} (\tilde{p} \frac{\partial p}{\partial z}) \right]. dV \end{aligned} \quad (2.7)$$

According to the divergence theorem, the integral of the normal component of a vector field $\vec{\phi}$, taken over a closed surface Ω , is equal to the integral of the divergence of the vector field, taken over the volume V , enclosed by the surface Ω ,

$$\int_V (\nabla \cdot \vec{\phi}). dV = \int_{\Omega} (\vec{\phi} \cdot \vec{n}). d\Omega \quad (2.8)$$

where \vec{n} is the unit normal vector with positive orientation away from the volume V .

Application of this theorem to the last integral term in Eq. (2.7) yields

$$\begin{aligned} \int_V \left[\frac{\partial}{\partial x} (\tilde{p} \frac{\partial p}{\partial x}) + \frac{\partial}{\partial y} (\tilde{p} \frac{\partial p}{\partial y}) + \frac{\partial}{\partial z} (\tilde{p} \frac{\partial p}{\partial z}) \right]. dV = \int_V (\nabla \cdot (\tilde{p} \nabla p)). dV = \\ \int_{\Omega} \left(\tilde{p} \frac{\partial p}{\partial n} \right). d\Omega = - \int_{\Omega} (j\rho_0 \omega \tilde{p} \vec{v} \cdot \vec{n}). d\Omega \end{aligned} \quad (2.9)$$

Substitution of Eq. (2.9) into Eq. (2.7) yields the 'weak form' of the weighted residual formulation of the Helmholtz equation,

$$\int_V (\nabla \tilde{p} \cdot \nabla p) dV - \omega^2 \int_V \left(\frac{1}{c^2} \tilde{p} p \right) dV = \int_V (j \rho_0 \omega \tilde{p} q) dV - \int_{\Omega} (j \rho_0 \omega \tilde{p} \vec{v} \cdot \vec{n}) d\Omega \quad (2.10)$$

2.3.2 Field variable approximations

In the finite element method, the fluid domain V is discretized into a number of small subdomains V_e ('finite elements') and a number of nodes, say n_e , are defined at some particular locations in each element. Within each element, the distribution of the field variable, i.e. the pressure p , is approximated as an expansion \hat{p} in terms of a number, say n_p , of prescribed shape functions N_i^e , which are only defined within the considered element domain V_e ,

$$p(x, y, z) \approx \hat{p}(x, y, z) = \sum_{i=1}^{n_p} N_i^e(x, y, z) \cdot a_i \quad (x, y, z) \in V_e \quad (2.11)$$

For the commonly used linear tetrahedral and linear hexahedral fluid elements, the nodes are defined at each corner point of their element volumes and the number of element shape functions is equal to the number of nodes ($n_p = n_e$). Each shape function N_i^e is defined, such that it has a value of unity at node i of the element and that it is zero at all other element nodes. In this way, each contribution a_i in the pressure expansion (2.11) represents the pressure approximation \hat{p}_i at node i of the element,

$$\hat{p}(x, y, z) = \sum_{i=1}^{n_e} N_i^e(x, y, z) \cdot \hat{p}_i \quad (x, y, z) \in V_e \quad (2.12)$$

Based on the element shape functions N_i^e , which are locally defined in one element V_e , some global shape functions N_i may be constructed, which are defined in the entire fluid domain V . In each element domain V_e to which node i belongs, the global shape function N_i is identical to the corresponding element shape function N_i^e , while it is zero in all other element domains. In this way, a global pressure expansion may be defined as

$$\hat{p}(x, y, z) = \sum_{i=1}^{n_f} N_i(x, y, z) \cdot \hat{p}_i = [N] \cdot \{\hat{p}_i\} \quad (x, y, z) \in V \quad (2.13)$$

where n_f is the total number of nodes in the discretization, $[N]$ is a $(1 \times n_f)$ vector of global shape functions and $\{\hat{p}_i\}$ is a $(n_f \times 1)$ vector of unknown nodal pressure values. The corresponding pressure gradient approximation becomes then

$$\bar{\nabla}p \approx \bar{\nabla}\hat{p} = \begin{bmatrix} \frac{\partial \hat{\Phi}}{\partial x} \\ \frac{\partial \hat{\Phi}}{\partial y} \\ \frac{\partial \hat{\Phi}}{\partial z} \end{bmatrix} = [\partial][N] \cdot \{\hat{p}_i\} = [B] \cdot \{\hat{p}_i\} \quad (2.14)$$

where $[\partial]$ is a (3×1) vector of gradient operators and $[B]$ is a $(3 \times n_f)$ matrix of gradient components of the global shape functions.

The concepts of element discretization and shape function definition are illustrated in Fig. 2.1 for a two-dimensional fluid volume, which is discretized into linear rectangular fluid elements.

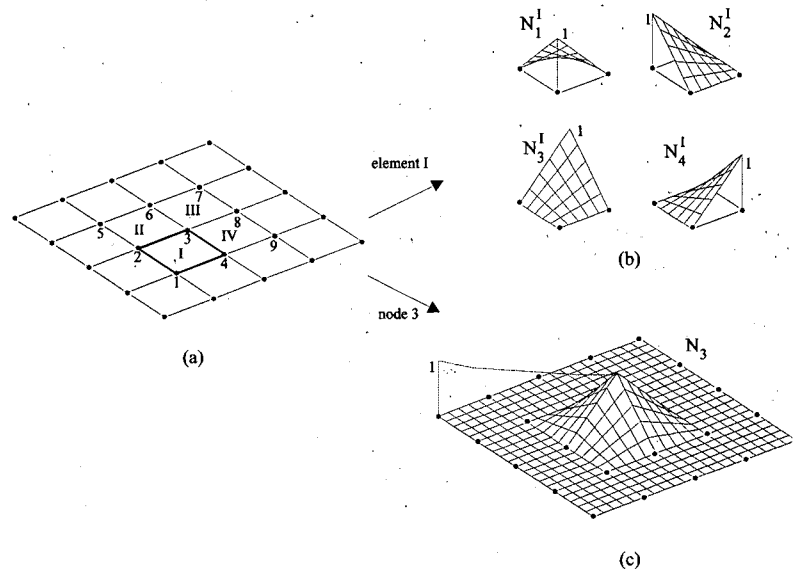


Fig. 2.1 : (a) FE discretization of a two-dimensional volume, (b) element shape functions, (c) global shape function

2.3.3 Finite element model for uncoupled acoustic problems

The determination of the unknown nodal pressure values \hat{p}_i in the expansions (2.13) and (2.14) is based on the weak form (2.10) of the weighted residual formulation of the Helmholtz equation.

In the most commonly used Galerkin weighted residual approach, the weighting function \tilde{p} and its gradient vector in Eq. (2.10) are expanded in terms of the same set of shape functions as used for the pressure and pressure gradient expansions, i.e.

$$\tilde{p}(x, y, z) = \sum_{i=1}^{n_f} N_i(x, y, z) \cdot \tilde{p}_i = [N] \cdot \{\tilde{p}_i\} \quad (x, y, z) \in V \quad (2.15)$$

$$\bar{\nabla}\tilde{p} = [\partial][N] \cdot \{\tilde{p}_i\} = [B] \cdot \{\tilde{p}_i\} \quad (2.16)$$

The substitution of the expansions (2.13)-(2.16) into the various integral terms of the weak form (2.10) of the weighted residual formulation enables the definition of an acoustic stiffness matrix (section 2.3.3.1), an acoustic mass matrix (section 2.3.3.2), acoustic excitation vectors (section 2.3.3.3) and an acoustic damping matrix (section 2.3.3.4). The combination of these components yields an acoustic finite element model (section 2.3.3.5.), which can be solved for the unknown nodal pressure values \hat{p}_i .

2.3.3.1 Acoustic stiffness matrix

For the first integral term in the left-hand side of Eq. (2.10), the substitutions yield

$$\begin{aligned} \int_V (\bar{\nabla} \tilde{p} \cdot \bar{\nabla} \hat{p}) \, dV &= \int_V \left(([B] \{ \tilde{p}_i \})^T \cdot ([B] \{ \hat{p}_i \}) \right) \, dV \\ &= \{ \tilde{p}_i \}^T \cdot \left(\int_V ([B]^T \cdot [B]) \, dV \right) \cdot \{ \hat{p}_i \} = \{ \tilde{p}_i \}^T \cdot [K] \cdot \{ \hat{p}_i \}, \end{aligned} \quad (2.17)$$

where $[.]^T$ denotes the transpose of a matrix and $[K]$ is a $(n_x n_y)$ matrix.

To preserve the analogy with a structural finite element model, the matrix $[K]$ is called the acoustic 'stiffness' matrix, although it represents an inverse mass or mobility matrix, relating the pressure to an acceleration.

The matrix element K_{ij} on row i and column j of this matrix is

$$K_{ij} = \int_V \left(\frac{\partial N_i}{\partial x} \frac{\partial N_j}{\partial x} + \frac{\partial N_i}{\partial y} \frac{\partial N_j}{\partial y} + \frac{\partial N_i}{\partial z} \frac{\partial N_j}{\partial z} \right) \, dV \quad (2.18)$$

Recall that the global shape functions N_i and N_j (and their spatial derivatives) have only non-zero values in the domains of those elements, to which, respectively, node i and node j belong. As a result, the volume integration in Eq. (2.18) may be confined to the integration over the domains of those elements, to which both node i and node j belong. Since the latter integration may be regarded as a sum of integrations over each of the common element domains and since the global shape functions in each of these element domains are identical to the corresponding element shape functions, matrix element K_{ij} may be expressed as

$$K_{ij} = \sum_{e=1}^{m_{ij}} \left(\int_{V_e} \left(\frac{\partial N_i^e}{\partial x} \frac{\partial N_j^e}{\partial x} + \frac{\partial N_i^e}{\partial y} \frac{\partial N_j^e}{\partial y} + \frac{\partial N_i^e}{\partial z} \frac{\partial N_j^e}{\partial z} \right) \, dV \right) \quad (2.19)$$

where m_{ij} is the number of elements, to which both node i and node j belong.

Since each node belongs to common elements with only a few, adjacent nodes, only a few matrix elements K_{ij} are non-zero. This results in a sparsely populated stiffness matrix $[K]$.

Due to this advantageous matrix property, the *practical calculation* of the stiffness matrix can be performed in a very efficient way. By confining the volume integration in Eq. (2.17) to one element domain, one may write

$$\begin{aligned} \int_{V_e} (\bar{\nabla} \tilde{p} \cdot \bar{\nabla} \hat{p}) \, dV &= \{ \tilde{p}_i^e \}^T \cdot \left(\int_{V_e} \left(([\partial] [N^e])^T \cdot ([\partial] [N^e]) \right) \, dV \right) \cdot \{ \hat{p}_i^e \} \\ &= \{ \tilde{p}_i^e \}^T \cdot \left(\int_{V_e} \left([B^e]^T \cdot [B^e] \right) \, dV \right) \cdot \{ \hat{p}_i^e \} = \{ \tilde{p}_i^e \}^T \cdot [K^e] \cdot \{ \hat{p}_i^e \}, \end{aligned} \quad (2.20)$$

where $[N^e]$ is a $(1 \times n_p)$ vector of element shape functions and $\{\hat{p}_i^e\}$ is a $(n_p \times 1)$ vector of unknown nodal pressure values of the considered element. The matrix elements in the associated $(n_p \times n_p)$ element stiffness matrix $[K^e]$ are

$$K_{ij}^e = \int_{V_e} \left(\frac{\partial N_i^e}{\partial x} \frac{\partial N_j^e}{\partial x} + \frac{\partial N_i^e}{\partial y} \frac{\partial N_j^e}{\partial y} + \frac{\partial N_i^e}{\partial z} \frac{\partial N_j^e}{\partial z} \right) dV \quad (2.21)$$

Note that, since all element shape functions have non-zero values in their element domain V_e , each element stiffness matrix is now fully populated.

The calculation of the global stiffness matrix $[K]$ may now be performed in a two-step procedure. In the first step, all element stiffness matrices are calculated. In the second step, each non-zero element K_{ij} of the global stiffness matrix is obtained, according to Eq. (2.19), from a simple addition of the corresponding entries Eq. (2.21) in the appropriate element stiffness matrices. With an appropriate numbering of the nodes in the FE discretization, the non-zero entries in the stiffness matrix appear in a narrow band around the matrix diagonal, yielding a sparsely populated, banded stiffness matrix.

2.3.3.2 Acoustic mass matrix

In a completely similar way, the second integral term in the left-hand side of Eq. (2.10) may be expressed as

$$\begin{aligned} -\omega^2 \int_V \left(\frac{1}{c^2} \tilde{p} \cdot \hat{p} \right) dV &= -\omega^2 \{\tilde{p}_i\}^T \cdot \left(\int_V \left(\frac{1}{c^2} [N]^T \cdot [N] \right) dV \right) \cdot \{\hat{p}_i\} \\ &= -\omega^2 \{\tilde{p}_i\}^T \cdot [M] \cdot \{\hat{p}_i\} \end{aligned} \quad (2.22)$$

where $[M]$ is a $(n_p \times n_p)$ matrix.

Again, to preserve the analogy with a structural finite element model, the matrix $[M]$ is called the acoustic 'mass' matrix, although it represents a compressibility matrix, relating the pressure to a displacement.

As for the global stiffness matrix, the *practical calculation* of this sparsely populated, banded global mass matrix is based on an assemblage of the element mass matrices, according to

$$M_{ij} = \int_V \left(\frac{1}{c^2} N_i N_j \right) dV = \sum_{e=1}^{m_{ij}} \left(\int_{V_e} \left(\frac{1}{c^2} N_i^e N_j^e \right) dV \right) \quad (2.23)$$

2.3.3.3 Acoustic excitation vectors

The first integral term in the right hand side of Eq. (2.10) may be expressed as

$$\int_V (j\rho_0\omega\tilde{p}q) dV = \{\tilde{p}_i\}^T \cdot \left(\int_V (j\rho_0\omega[N]^T q) dV \right) = \{\tilde{p}_i\}^T \cdot \{Q_i\} \quad (2.24)$$

where $\{Q_i\}$ is a $(n_p \times 1)$ **acoustic source vector**.

When the distribution q of external acoustic sources is confined, for instance, to an acoustic point source of strength \bar{q}_i , located at node i , the source distribution q is

$$q(x, y, z) = \bar{q}_i \cdot \delta(x_i, y_i, z_i) \quad (2.25)$$

where δ is a Dirac delta function at node i . The subsequent source vector becomes then

$$\{Q_i\} = j\rho_0\omega \left(\int_V (\bar{q}_i \cdot [N]^T \cdot \delta) dV \right) \quad (2.26)$$

Provided that node i is not located on the boundary surface of V , all components of the $(n \times 1)$ source vector are zero, except the component on row i , which equals $j\rho_0\omega\bar{q}_i$.

The second integral term in the right hand side of Eq. (2.10) allows the introduction of the boundary conditions. Since the integration over the boundary surface Ω may be regarded as a sum of the integrations over the subsurfaces Ω_v , Ω_z and Ω_p and since the normal velocity and normal impedance boundary conditions (2.3) and (2.4) must be satisfied on, respectively, Ω_v and Ω_z , the second integral term in the right hand side of Eq. (2.10) may be expressed as

$$- \int_{\Omega_v} (j\rho_0\omega\bar{p}\bar{v}_n) d\Omega - \int_{\Omega_p} (j\rho_0\omega\bar{p}\bar{v} \cdot \bar{n}) d\Omega - \int_{\Omega_z} (j\rho_0\omega\bar{p}\bar{A}\hat{p}) d\Omega \quad (2.27)$$

The substitution of expansion (2.15) into the first term of Eq. (2.27) yields

$$- \int_{\Omega_v} (j\rho_0\omega\bar{p}\bar{v}_n) d\Omega = \{\bar{p}_i\}^T \left(\int_{\Omega_v} (-j\rho_0\omega[N]^T \bar{v}_n) d\Omega \right) = \{\bar{p}_i\}^T \{V_{ni}\} \quad (2.28)$$

The component on row i of the $(n \times 1)$ **input velocity vector** $\{V_{ni}\}$ is thus

$$V_{ni} = \int_{\Omega_v} (-j\rho_0\omega N_i \bar{v}_n) d\Omega \quad (2.29)$$

The boundary surface of an element is the union of all its faces. The boundary surface of a linear tetrahedral or a linear hexahedral fluid element, for instance, is the union of, respectively, four and six faces. For these compatible elements, the value of a global shape function N_i at a certain element face is only non-zero, if node i is located on the considered element face. As a consequence, the value of a global shape function N_i at the boundary surface Ω_v and the subsequent vector component V_{ni} are only non-zero for those nodes that are located on the boundary surface Ω_v .

Hence, the *practical calculation* of the input velocity vector is based on its component expression

$$V_{ni} = -j\rho_0\omega \sum_{e=1}^{m_{vi}} \sum_{f=1}^{f_{vi}^e} \left(\int_{\Omega_e^f} (N_i^e \cdot \bar{v}_n) d\Omega \right), \quad (2.30)$$

where m_{vi} is the number of elements, for which node i is located on their f_{vi}^e element faces Ω_e^f , that are part of the boundary surface Ω_v .

The prescribed normal velocity at a certain location in an element face is often specified by a shape function expansion, comparable to the pressure expansion (2.13),

$$\bar{v}_n(x, y, z) = \{n\}^T \cdot [N_{ve}^f] \cdot \{\bar{v}_e^f\} \quad (x, y, z) \in \Omega_e^f \quad (2.31)$$

where the (3×1) vector $\{n\}$ consists of the x -, y - and z -components of the unit vector, normal to the considered element face. The matrix

$$[N_{ve}^f] = \begin{bmatrix} N_1^e & 0 & 0 & \dots & N_{n_v}^e & 0 & 0 \\ 0 & N_1^e & 0 & \dots & 0 & N_{n_v}^e & 0 \\ 0 & 0 & N_1^e & \dots & 0 & 0 & N_{n_v}^e \end{bmatrix} \quad (2.32)$$

is a $(3 \times 3n_v)$ matrix, which contains the pressure shape functions of the n_v nodes, located on the considered element face. In each of these nodes, the x -, y - and z -component of the fluid velocity is specified, yielding the $(3n_v \times 1)$ vector

$$\{\bar{v}_e^f\}^T = \{\bar{v}_{x1} \quad \bar{v}_{y1} \quad \bar{v}_{z1} \quad \dots \quad \bar{v}_{xn_v} \quad \bar{v}_{yn_v} \quad \bar{v}_{zn_v}\} \quad (2.33)$$

The substitution of expansion (2.15) into the second term of Eq. (2.27) yields

$$- \int_{\Omega_p} (j\rho_0\omega\bar{p}\bar{v}\cdot\bar{n}) \cdot d\Omega = \{\tilde{p}_i\}^T \cdot \left(\int_{\Omega_p} (-j\rho_0\omega[N]^T\bar{v}\cdot\bar{n}) \cdot d\Omega \right) = \{\tilde{p}_i\}^T \cdot \{P_i\} \quad (2.34)$$

Due to the particular shapes of the global shape functions N_i , the component on row i of the $(n_i \times 1)$ **input pressure vector** $\{P_i\}$,

$$P_i = \int_{\Omega_p} (-j\rho_0\omega N_i\bar{v}\cdot\bar{n}) \cdot d\Omega \quad (2.35)$$

is only non-zero, if node i is located on the boundary surface Ω_p . Since the latter expression doesn't allow the introduction of the prescribed pressure boundary condition (2.2), this boundary condition enters the finite element model in a different way, as will be discussed in section 2.3.3.5.

2.3.3.4 Acoustic damping matrix

The third term in Eq. (2.27) may be expressed as

$$\begin{aligned} - \int_{\Omega_z} (j\rho_0\omega\bar{p}\bar{A}\hat{p}) \cdot d\Omega &= -j\omega\{\tilde{p}_i\}^T \cdot \left(\int_{\Omega_z} (\rho_0\bar{A}[N]^T \cdot [N]) \cdot d\Omega \right) \cdot \{\hat{p}_i\} \\ &= -j\omega\{\tilde{p}_i\}^T \cdot [C] \cdot \{\hat{p}_i\} \end{aligned} \quad (2.36)$$

where $[C]$ is the $(n_f \times n_f)$ acoustic damping matrix, induced by the impedance boundary conditions.

The matrix element C_{ij} on row i and column j of this matrix is

$$C_{ij} = \int_{\Omega_z} (\rho_0\bar{A}N_iN_j) \cdot d\Omega \quad (2.37)$$

As it is the case for the stiffness and mass matrix, the damping matrix is sparsely populated, since matrix element C_{ij} is only non-zero, if node i and node j are located on at least one common element face that is part of the boundary surface Ω_z .

The *practical calculation* of the non-zero matrix elements is therefore based on the expression

$$C_{ij} = \sum_{f=1}^{m_{zij}} \left(\int_{\Omega_f^e} (\rho_0\bar{A}N_i^e N_j^e) \cdot d\Omega \right) \quad (2.38)$$

where m_{zij} is the number of element faces Ω_e^f , on which both node i and node j are located and that are part of the boundary surface Ω_Z . The specification of the prescribed normal admittance is usually restricted to a constant value per element face in Ω_Z .

2.3.3.5 Acoustic finite element model

By substituting expressions (2.17), (2.22), (2.24), (2.28), (2.34) and (2.36) into Eq. (2.10), the weak form of the weighted residual formulation of the Helmholtz equation, including the boundary conditions (2.3) and (2.4), becomes

$$\{\tilde{p}_i\}^T \cdot ([K] + j\omega[C] - \omega^2[M]) \cdot \{\hat{p}_i\} = \{\tilde{p}_i\}^T \cdot (\{Q_i\} + \{V_{ni}\} + \{P_i\}) \quad (2.39)$$

Since the weighted residual formulation should hold for any expansion of the weighting function, i.e. for any set of shape function contributions $\{\tilde{p}_i\}$ (see Eq. (2.15)), a set of n_f equations in the n_f unknown nodal pressure approximations \hat{p}_i is obtained,

$$([K] + j\omega[C] - \omega^2[M]) \cdot \{\hat{p}_i\} = \{Q_i\} + \{V_{ni}\} + \{P_i\} \quad (2.40)$$

Row i in this matrix equation expresses the weighted residual formulation, in which the global shape function N_i , associated with node i , is used as weighting function \tilde{p} .

The prescribed pressure boundary condition (2.2) is not yet included in matrix Eq. (2.40). This is usually done by directly assigning the prescribed pressure value at each node location on the boundary surface Ω_p to its corresponding nodal unknown \hat{p}_i .

When this assignment is done for the $n_{\bar{p}}$ nodes on Ω_p , only $n_a (= n_f - n_{\bar{p}})$ pressure approximations \hat{p}_i are still unknown. This means that $n_{\bar{p}}$ equations should be eliminated in matrix Eq. (2.40) to have a well-determined set of equations.

This is usually done by eliminating each row in Eq. (2.40), that expresses the weighted residual formulation, in which the global shape function of a node on the boundary surface Ω_p is used as weighting function. The elimination of these equations, which orthogonalize the error on the pressure predictions in the region near the boundary surface Ω_p with respect to the shape functions in this region, is motivated by the fact that this prediction error is smaller than the errors in the other regions of the fluid domain, since the exact pressure values at the nodes of the boundary surface Ω_p are a priori assigned.

By eliminating the appropriate rows in Eq. (2.40) and by shifting all terms in the left hand side of Eq. (2.40), which contain the a priori assigned nodal pressure values, to the right hand side vector, the resulting finite element model for an uncoupled acoustic problem is obtained,

$$\boxed{([K_a] + j\omega[C_a] - \omega^2[M_a]) \cdot \{p_i\} = \{F_{ai}\}} \quad (2.41)$$

where the $(n_a \times 1)$ vector $\{p_i\}$ contains the remaining unknown nodal pressure approximations and where the acoustic stiffness, damping and mass matrices $[K_a]$, $[C_a]$ and $[M_a]$ are now $(n_a \times n_a)$ matrices.

Since the non-zero components of $\{p_i\}$ occur only in the eliminated equations of Eq. (2.40), the $(n_a \times 1)$ acoustic force vector $\{F_{ai}\}$ contains the stiffness,

damping and mass terms in the a priori assigned nodal pressures and the contributions from the acoustic source vector (2.24) and the input velocity vector (2.28).

2.4 Convergence and parametric mapping

2.4.1 Convergence

The prediction accuracy, obtained from a finite element model, depends mainly on the number of elements and on the nature of the prescribed shape functions. In this framework, it is important that the accuracy systematically improves as the number of elements increases, so that the proposed solution expansion eventually converges towards the exact solution. To ensure this convergence, some conditions must be satisfied by the shape functions and the weighting functions.

A necessary condition for the solution expansion (2.13) to be convergent is the condition of **completeness**.

The unknown nodal pressure degrees of freedom result from the matrix Eq. (2.41), in which the coefficients are defined in integral forms. All terms in the integration functions, which originate from the weighted residual formulation (2.10), comprise the pressure field p , the weighting function \tilde{p} and/or their first-order spatial derivatives (gradient vectors).

In the exact solution, the pressure field and its gradient vector components - and hence each of the integration terms in Eq. (2.10) - reach constant values within any infinitesimally small region in the fluid domain. Therefore, a necessary convergence condition upon the element shape functions is that the approximating pressure expansion (2.13) and the pressure gradient expansion (2.14) can also reach constant values within each element.

A second convergence consideration concerns the element **compatibility**. In order to be able to evaluate the various integrals in the weighted residual formulation (2.10), shape functions (and weighting functions), which would result in terms in the integrals becoming infinite, must be avoided. To achieve this, the acoustic elements should be compatible in that the first-order pressure derivatives, being the highest-order derivatives in the weighted residual formulation (2.10), exist for the proposed pressure expansion (2.13) within each element and that this pressure expansion is continuous along the interelement boundaries. Acoustic elements, that yield a pressure expansion, which is continuous along the interelement boundaries, but whose first-order derivatives are discontinuous along the interelement boundaries, are denoted as elements with C^0 -continuity.

For a finite element discretization that consists of conforming elements, i.e. elements that satisfy both the completeness and compatibility conditions, the solution expansion converges monotonically to the exact solution. For a finite element discretization that consists of nonconforming elements, i.e. elements that

satisfy the completeness condition but not the compatibility condition, its - not necessarily monotonic - convergence can still be ensured, provided that the discretization passes a 'patch test', which is basically a completeness test on an assemblage of incompatible elements.

Since the differentiation and integration of a polynomial function are very easy, the construction of a finite element model becomes simple and straightforward, if the element shape functions are obtained from a set of polynomial functions. For this type of finite element discretizations, some specific requirements may be derived from the above mentioned convergence considerations. As mentioned before, the highest-order spatial derivatives of the pressure p and the weighting function \tilde{p} in the weighted residual formulation (2.10) are of first order. Hence, the convergence of an acoustic finite element discretization is ensured, if the expansions (2.13) and (2.15) for, respectively, p and \tilde{p} consist of polynomial shape functions, which are complete up to at least the first order within each element and if they are continuous along the interelement boundaries (C^0 -continuity).

Commonly used elements in acoustic finite element modeling are linear rectangular and linear triangular elements for two-dimensional problems and linear rectangular prism and linear tetrahedral elements for three-dimensional problems (see Fig. 2.2).

The pressure shape functions for these elements are defined as follows :

- linear rectangular element (Fig. 2.2 (a))

$$N_i^e = \frac{1}{4}(1 + \xi_i \xi)(1 + \eta_i \eta) \quad (i = 1..4) \quad (2.42)$$

- linear triangular element (Fig. 2.2 (b))

$$N_i^e = L_i \quad (i = 1..3) \quad (2.43)$$

where the normalized area co-ordinate system (L_1, L_2, L_3) is related to the global Cartesian co-ordinate system (x, y) :

$$\begin{Bmatrix} L_1 \\ L_2 \\ L_3 \end{Bmatrix} = \frac{1}{2\Delta} \begin{bmatrix} b_1 & c_1 & a_1 \\ b_2 & c_2 & a_2 \\ b_3 & c_3 & a_3 \end{bmatrix} \begin{Bmatrix} x \\ y \\ 1 \end{Bmatrix} \quad (2.44)$$

where

$$\Delta = \frac{1}{2} \det \begin{bmatrix} 1 & x_1 & y_1 \\ 1 & x_2 & y_2 \\ 1 & x_3 & y_3 \end{bmatrix}, \quad (2.45)$$

$$a_1 = x_2 y_3 - x_3 y_2, \quad b_1 = y_2 - y_3, \quad c_1 = x_3 - x_2$$

The other parameters are obtained from cyclic rotation of the indices.

- linear rectangular prism element (Fig. 2.2 (c))

$$N_i^e = \frac{1}{8}(1 + \xi_i \xi)(1 + \eta_i \eta)(1 + \zeta_i \zeta) \quad (i = 1..8) \quad (2.46)$$

- linear tetrahedral element (Fig. 2.2 (d))

$$N_i^e = L_i \quad (i = 1..4) \quad (2.47)$$

where the normalized volume co-ordinate system (L_1, L_2, L_3, L_4) is related to the global Cartesian co-ordinate system (x, y, z) in a similar way as the relations (2.44) and (2.45) for the normalized area co-ordinate system.

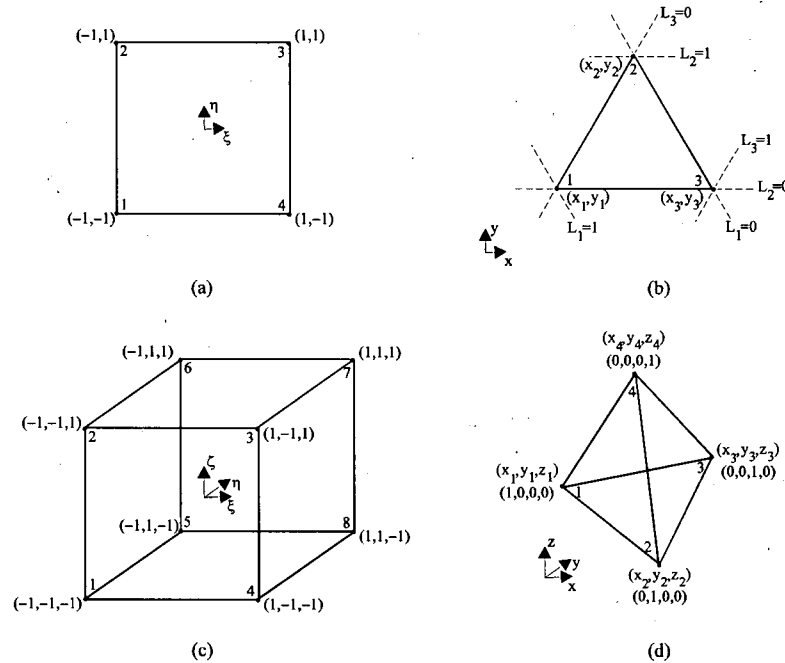


Fig. 2.2: linear rectangular (a), linear triangular (b), linear rectangular prism (c) and linear tetrahedral (d) elements

The convergence of a finite element discretization with these element types is ensured. All these elements satisfy the necessary completeness condition, since the polynomial shape functions comprise at least all terms up to the first order. The efficiency of triangular and tetrahedral elements may be noticed in this respect, since their number of nodes equals the minimum number, required for a complete first-order polynomial expansion.

All elements satisfy also the C^0 -continuity condition, since the pressure in each element boundary is completely defined by the pressure degrees of freedom of the nodes in that boundary. For the linear rectangular element (see Fig. 2.2 (a)), for instance, the pressure approximation is

$$\begin{aligned}
 p &\approx N_1^e \cdot p_1 + N_2^e \cdot p_2 + N_3^e \cdot p_3 + N_4^e \cdot p_4 \\
 &\approx \left(\frac{p_1 + p_2 + p_3 + p_4}{4} \right) + \left(\frac{p_3 + p_4 - p_1 - p_2}{4} \right) \cdot \xi + \left(\frac{p_2 + p_3 - p_1 - p_4}{4} \right) \cdot \eta \\
 &\quad + \left(\frac{p_1 + p_3 - p_2 - p_4}{4} \right) \cdot \xi \eta
 \end{aligned} \tag{2.48}$$

The pressure approximation along the boundary between nodes 3 and 4 (i.e. $\xi=1, \eta \in [-1, 1]$) has a linear shape,

$$p(1, \eta) = \left(\frac{p_3 + p_4}{2} \right) + \left(\frac{p_3 - p_4}{2} \right) \cdot \eta \tag{2.49}$$

which is uniquely defined by the pressure values at nodes 3 and 4. Since in the adjacent rectangular element the pressure along this boundary has also a linear

shape, which is uniquely defined by the common nodes 3 and 4, the pressure continuity along this boundary is ensured.

2.4.2 Parametric mapping

To obtain a convergent discretization with elements, having polynomial element shape functions, the faces of the element boundary surfaces must usually be located in 'planes', having a constant value for one of the Cartesian co-ordinates or one of the normalized area or volume co-ordinates. As a result, a convergent discretization with polynomial shape functions is usually confined to rectangular and triangular elements for two-dimensional problems and rectangular prism and tetrahedral elements for three-dimensional problems, as discussed in the previous section.

For most acoustic problems, however, the fluid domain has a geometrically complex shape, which cannot be discretized exactly into an assemblage of these geometrically simple elements. Consequently, a finite element discretization for such problems induces not only an approximation error on the acoustic pressure predictions, but also on the geometrical description. To keep the geometrical discretization error within acceptable levels, a discretization is often constructed using the concept of *parametric mapping*, which enables the use of elements with more complex, distorted geometries.

The above mentioned geometrically simple elements, denoted as 'parent' elements, constitute the starting point of the mapping concept. In these parent elements, for which convergence is ensured, the pressure field is described in terms of polynomial shape functions, which are defined in a local element co-ordinate system (Cartesian, normalized area or normalized volume co-ordinate system). By distorting such a parent element, together with its local element co-ordinate system, an element with a distorted geometry and a local, now curvilinear, element co-ordinate system is obtained.

In a similar way as for the pressure approximation, the geometry of the distorted element, i.e. the relationship between the global Cartesian and the local curvilinear co-ordinates of each point in the distorted element domain, is described as an expansion of some prescribed shape functions. For some points in the element*, their desired global co-ordinates are specified. By defining each shape function as a (polynomial) function in the local co-ordinate system with a value of unity at one of the specified points and zero at the others, each shape function contribution in the geometrical expansion corresponds with the desired global Cartesian co-ordinates of one of the specified points.

Elements with the same shape functions, describing their geometry and their pressure distributions, are commonly used and denoted as isoparametric acoustic elements. Provided that some limitations on the amount of distortion are not violated, the parametric mapping concept yields a one-to-one correspondence between the global Cartesian and the local curvilinear co-ordinate systems. An important feature of this type of isoparametric mapping is that the convergence properties of the parent discretization are usually preserved in the mapped discretization.

Linear quadrilateral and linear hexahedral elements, for instance, are commonly used acoustic finite elements, which are obtained from an isoparametric mapping of, respectively, the linear rectangular and the linear rectangular prism elements. The geometry of these isoparametric elements, i.e.

* the specified points usually coincide with (some of) the nodes of the element and their number equals the number of prescribed shape functions

the relation between the global Cartesian co-ordinates (x, y, z) of each point in the element and the corresponding local co-ordinates (ξ, η, ζ) , is expressed as

$$\begin{aligned} x(\xi, \eta, \zeta) &= \sum_{i=1}^{n_e} N_i^e(\xi, \eta, \zeta) \cdot x_i = [N^e(\xi, \eta, \zeta)] \{x_i\} \\ y(\xi, \eta, \zeta) &= \sum_{i=1}^{n_e} N_i^e(\xi, \eta, \zeta) \cdot y_i = [N^e(\xi, \eta, \zeta)] \{y_i\} \\ z(\xi, \eta, \zeta) &= \sum_{i=1}^{n_e} N_i^e(\xi, \eta, \zeta) \cdot z_i = [N^e(\xi, \eta, \zeta)] \{z_i\} \end{aligned} \quad (2.50)$$

where N_i^e are the parent element shape functions (see Eq. (2.42) and (2.46)) and where x_i, y_i, z_i are the desired global Cartesian co-ordinates of the element nodes.

Fig. 2.3 illustrates this concept for the isoparametric mapping of a linear rectangular parent element onto a linear quadrilateral element.

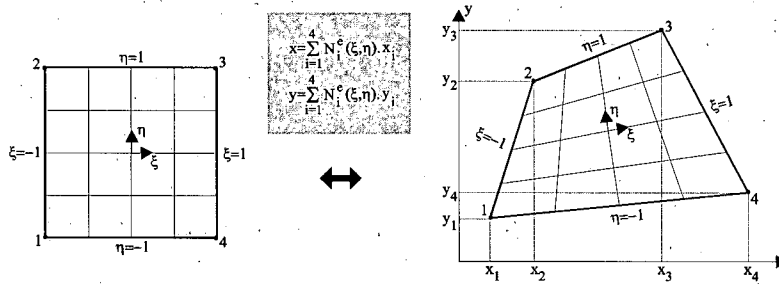


Fig. 2.3: isoparametric linear quadrilateral element

Based on the co-ordinate transformation of type (2.50), the integration functions in the weighted residual formulation (2.10) may be transformed from the global Cartesian to the local curvilinear co-ordinates. Due to the simple geometry of the parent elements, the integration limits of the resulting integrals, which could be complicated when defined in the global Cartesian co-ordinates, become constant in the local co-ordinates. Therefore, the co-ordinate transformation is a useful tool for the practical calculation of the finite element model (2.41).

According to the rules of partial differentiation, the spatial derivatives with respect to the local element co-ordinates ξ, η and ζ may be expressed in terms of those with respect to the global Cartesian co-ordinates x, y and z ,

$$\begin{bmatrix} \frac{\partial N_i^e}{\partial \xi} \\ \frac{\partial N_i^e}{\partial \eta} \\ \frac{\partial N_i^e}{\partial \zeta} \end{bmatrix} = \begin{bmatrix} \frac{\partial x}{\partial \xi} & \frac{\partial y}{\partial \xi} & \frac{\partial z}{\partial \xi} \\ \frac{\partial x}{\partial \eta} & \frac{\partial y}{\partial \eta} & \frac{\partial z}{\partial \eta} \\ \frac{\partial x}{\partial \zeta} & \frac{\partial y}{\partial \zeta} & \frac{\partial z}{\partial \zeta} \end{bmatrix} \begin{bmatrix} \frac{\partial N_i^e}{\partial x} \\ \frac{\partial N_i^e}{\partial y} \\ \frac{\partial N_i^e}{\partial z} \end{bmatrix} = [J(\xi, \eta, \zeta)] \begin{bmatrix} \frac{\partial N_i^e}{\partial x} \\ \frac{\partial N_i^e}{\partial y} \\ \frac{\partial N_i^e}{\partial z} \end{bmatrix} \quad (2.51)$$

Each element in the Jacobian matrix $[J]$ is a function in the local element co-ordinates ξ, η and ζ , which is obtained from the mapping relationship (2.50). Based on the expressions (2.50) and (2.51), the integration variables in the integrals, which determine the components of the force vector and the stiffness, mass and damping matrix of the finite element model (2.41), may be transformed from the global Cartesian to the local element co-ordinates. This co-ordinate

transformation yields, for instance, for an element stiffness matrix, as defined in (2.20),

$$\begin{aligned} [K^e] &= \int_{V_e} \left(([\partial][N^e])^T \cdot ([\partial][N^e]) \right) dx dy dz \\ &= \int_{-1}^1 \int_{-1}^1 \int_{-1}^1 \left(([\partial][N^e])^T \cdot ([\partial][N^e]) \right) \det(J) d\xi d\eta d\zeta. \end{aligned} \quad (2.52)$$

in which the components of vector $[\partial]$, which are the partial differential operators with respect to the global co-ordinates x , y and z , are expressed in terms of the partial differential operators with respect to the local element co-ordinates ξ , η and ζ , using the inverse of the Jacobian matrix (see (2.51)).

2.5 Properties

Several advantageous properties of the stiffness, mass and damping matrices of an acoustic finite element model (2.41) may be derived from their element expressions.

- As already mentioned before, the matrices are ***sparsely populated*** due to the local character of the shape functions. Moreover, with an appropriate numbering of the nodes in the discretization, which is automatically generated in commercial FE programs, the matrices may have a ***banded*** structure, i.e the non-zero matrix elements may be arranged in a narrow band around the matrix diagonal.
- Since the indices i and j in the element expressions (2.18), (2.23) and (2.37) may be interchanged, the matrices are ***symmetrical***. This property is beneficial, not only for the required memory resources, since only half of the matrices must be stored, but also for the computational costs, since efficient symmetric matrix solvers can be used for solving the finite element model.
- Since the shape functions are independent of frequency, the elements of the stiffness and mass matrices are ***frequency independent***. This allows the use of standard eigenvalue solvers for the calculation of the undamped natural frequencies and mode shapes of structural and acoustic system (cf. section 2.6.2).
Although the frequency doesn't occur in an explicit way in (2.37), the elements of the damping matrix are usually frequency dependent, due to the frequency dependence of the prescribed normal impedance (or admittance).
- Since all element shape functions have real values, the elements of the stiffness and mass matrices are ***real***, while the elements of the damping matrix are usually complex, since the prescribed normal impedance (or admittance) is usually a complex function.
- The ***numerical calculation*** of the matrix coefficients is very ***easy*** and straightforward. The involved numerical integrations are usually performed with a simple Gauss quadrature rule with only a few integration points per element (see e.g. [2.52]).

- The finite element method can easily handle problems with **inhomogeneous** acoustic domains, in that the fluid properties in the various element domains can be different.

The modeling concepts, especially the use of (low-order) polynomial shape functions in the parent element definition, induce also some disadvantageous properties of the finite element method.

- The dynamic response of an acoustic system results from a complex mechanism of wave propagation in the fluid domain. The resulting spatial variation of the oscillatory dynamic response is mainly determined by the spatial distribution of the external source excitation and its frequency contents. The latter is caused by the fact that the acoustic wavelength λ depends on the frequency ω , i.e. $\lambda = 2\pi c / \omega = c / f$.

Since the (low-order) polynomial functions, used for the description of the pressure field, can only represent a restricted spatial variation, a large number of elements is required to accurately represent the oscillatory wave nature of the acoustic response.

To obtain an acceptable level of prediction accuracy, a general rule of thumb states that at least 10 elements per acoustic wavelength are required (see e.g. [2.49]). Hence, according to this rule of thumb, the number of elements should increase as the frequency increases, since the acoustic wavelength decreases as the frequency increases. Therefore, the larger the fluid domain and the higher the excitation frequency, the larger becomes the model size.

As a result, the application of the finite element method for real-life engineering problems usually involves **large model sizes** and requires a **large amount of memory and computational efforts** for constructing and solving the model.

As a result, the applicability of the finite element method is practically restricted to a **limited frequency range**. Above a certain frequency limit, which depends on the nature of the problem and on the available computer resources, these prediction methods would require a prohibitively large amount of computational effort and memory resources to get an acceptable level of accuracy.

- The prediction **accuracy for derived secondary field variables is smaller** than for primary field variables. Predictions of dynamic quantities such as fluid velocities or acoustic intensities are obtained by deriving the prediction results of the primary field variables, i.e. the acoustic pressure. Since the latter are usually expressed in terms of polynomial expansions, which are complete up to a certain order, the derived variables are expressed in terms of polynomial expansions, which are only complete up to a lower order. As a result, these lower-order polynomial expansions represent a smaller spatial variation of the derived secondary variables than the expansions of the corresponding primary variables.

In a linear hexahedral fluid element, for example, the pressure is expressed in terms of a polynomial expansion, which is complete up to the first order, while the fluid velocity vector, which is proportional to the spatial gradient of the pressure, is no longer expressed in terms of a complete linear expansion. However, there is no physical justification for the subsequent smaller spatial variation of the fluid velocity predictions, since the pressure and fluid velocity of an acoustic wave have the same spatial variation. Consequently, the prediction accuracy of the fluid velocity is smaller than the accuracy of the pressure for a given finite element discretization. Moreover, for low-order polynomial expansions of the primary field variables, the subsequent expansions for the derived secondary variables become often discontinuous at the interelement boundaries. This is the case, for example, for the fluid velocity in linear hexahedral fluid elements.

- Since the element domains in a finite element discretization have a finite volume and since only models of finite size are amenable to numerical solution algorithms, the finite element method is, in principle, restricted to acoustic problems, which are defined in **bounded fluid domains**. However, there are several ways to extend the modeling concepts of the finite element method to the use for solving acoustic problems with unbounded fluid domains, as discussed in section 2.7.

2.6 Solution methods

2.6.1 Direct solution method

In the direct solution method, the finite element model (2.41) is directly solved at each frequency of interest for the vector of unknown nodal pressures. Back-substitution of the solution vector into the pressure expansion (2.13) yields the finite element approximation for the steady-state acoustic pressure field.

In this respect, it can be noted that, due to the advantageous matrix properties of a finite element model (symmetry, frequency independence, ... (cf. section 2.5)), the main part of the computational efforts is spent on solving the (large) matrix equation (2.41), while the construction of the model, i.e. the calculation of the matrix elements, requires only some minor efforts.

2.6.2 Modal solution method

As already mentioned in section 2.5, the application of the finite element method for real-life engineering problems usually involves large model sizes and requires a large amount of memory and computational efforts. However, the model sizes and subsequent computational efforts may be substantially reduced by using the modal expansion technique.

In this technique, the acoustic pressure field is expanded in terms of (some of) the modes of the considered system. The contributions of the modes to the acoustic response become then the unknowns of the modal model instead of the nodal degrees of freedom in the original model.

Such a modal solution procedure consists mainly of the following steps:

1. calculation of the undamped acoustic modes:

The calculation of the undamped mode shapes of an interior acoustic system, in which the entire boundary surface is assumed to be perfectly rigid, are obtained by discarding the damping matrix $[C_a]$ and the external excitation vector $\{F_a\}$ in the finite element model (2.41). Since the stiffness and mass matrices $[K_a]$ and $[M_a]$ are independent of frequency, the mode shape predictions are obtained from the following eigenvalue problem,

$$[K_a]\{\Phi_m\} = \omega_m^2 [M_a]\{\Phi_m\} \quad (m = 1..n_a) \quad (2.53)$$

where each $(n_a \times 1)$ eigenvector $\{\Phi_m\}$ represents a mode shape and where the associated eigenvalue corresponds with the square of the natural frequency ω_m of that mode.

Note that, due to the discretization of the acoustic system, which has an infinite number of degrees of freedom and, hence, an infinite number of modes, into a system with n_a degrees of freedom, only n_a mode shapes are obtained.

2. projection onto a modal base :

The nodal degrees of freedom in the $(n_a \times 1)$ vector $\{p_i\}$ in the finite element model (2.41) are expressed in terms of a set of $m_a (\leq n_a)$ modal vectors,

$$\{p_i\} = \sum_{m=1}^{m_a} \phi_m \cdot \{\Phi_m\} = [\Phi] \cdot \{\phi_m\} \quad (2.54)$$

where $[\Phi]$ is a $(n_a \times m_a)$ matrix of modal vectors and where $\{\phi_m\}$ is a $(m_a \times 1)$ vector of modal participation factors.

3. modal model :

By substituting the modal expansion (2.54) into the finite element model (2.41) and by premultiplying both sides of the resulting matrix equation with the transpose of the modal vector matrix, the following modal model is obtained,

$$\left([\tilde{K}_a] + j\omega[\tilde{C}_a] - \omega^2[\tilde{M}_a] \right) \{\phi_m\} = \{\tilde{F}_a\} \quad (2.55)$$

where the $(m_a \times 1)$ modal excitation vector is

$$\{\tilde{F}_a\} = [\Phi]^T \{F_{ai}\} \quad (2.56)$$

and where the $(m_a \times m_a)$ modal stiffness, mass and damping matrices are

$$[\tilde{K}_a] = [\Phi]^T [K_a] [\Phi], \quad [\tilde{M}_a] = [\Phi]^T [M_a] [\Phi], \quad [\tilde{C}_a] = [\Phi]^T [C_a] [\Phi] \quad (2.57)$$

Due to the orthogonality of the modal vectors with respect to the mass matrix,

$$\{\Phi_{m_1}\}^T [M_a] \{\Phi_{m_2}\} = 0, \quad \text{if } m_1 \neq m_2, \quad (2.58)$$

the modal mass and modal stiffness matrices are diagonal matrices. By normalizing the modal vectors, according to

$$\{\Phi_{m_1}\}^T [M_a] \{\Phi_{m_1}\} = 1, \quad (m_1 = 1..m_a), \quad (2.59)$$

the modal mass matrix becomes the unity matrix,

$$[\tilde{M}_a] = \begin{bmatrix} 1 & & \\ & \ddots & \\ & & 1 \end{bmatrix} \quad (2.60)$$

and the diagonal modal stiffness matrix becomes

$$[\tilde{K}_a] = \begin{bmatrix} \omega_1^2 & & \\ & \ddots & \\ & & \omega_{m_a}^2 \end{bmatrix} \quad (2.61)$$

When the finite element model (2.41) has a proportional damping matrix, i.e. a damping matrix, which may be written as a linear combination of the stiffness and mass matrix,

$$[C_a] = \alpha[K_a] + \beta[M_a] \quad (2.62)$$

the modal damping matrix is also a diagonal matrix,

$$[\tilde{C}_a] = \begin{bmatrix} 2\zeta_1 \omega_1 & & \\ & \ddots & \\ & & 2\zeta_{m_a} \omega_{m_a} \end{bmatrix} \quad (2.63)$$

with the modal damping ratio's

$$\zeta_m = \frac{\alpha \omega_m}{2} + \frac{\beta}{2\omega_m} \quad (2.64)$$

4. solving the modal model :

The modal model (2.55) is solved at each frequency of interest for the vector $\{\phi_m\}$ of unknown modal participation factors. Back-substitution of the solution vector into the pressure expansion (2.13), taking into account the modal projection (2.54), yields the approximation for the steady-state acoustic pressure field,

$$p(x, y, z) \approx [N]\{p_i\} = [N][\Phi]\{\phi_m\} \quad (2.65)$$

Although all modes should be used ($m_a = n_a$) in the modal expansion (2.54) to get the same accuracy as with the direct solution method*, a relatively small truncated set of modes yields already a level of accuracy close to the one of the much larger original model. In this framework, a rule of thumb states that an accurate prediction of the steady-state dynamic behavior in a certain frequency range is obtained by using all modes with natural frequencies, smaller than twice the upper frequency limit of the considered frequency range.

In this way, a significant model size reduction can be obtained ($m_a \ll n_a$), especially in the low-frequency range, where the modal densities are small. In addition to the reduced model size, the matrices in a modal model often become diagonal, due to the orthogonality properties of the modes. As a result, when the steady-state response is needed at a large number of frequencies, the computational effort for constructing the modal base and then solving the reduced modal model at each frequency of interest is usually substantially smaller than for directly solving the original model at each frequency.

2.7 Exterior radiation problems

In principle, the finite element method can only be used for interior acoustic problems, which have a bounded acoustic domain, since the numerical implementation requires a finite number of finite elements. There are several ways, however, to extend the modeling concepts of the finite element method to the use for solving exterior acoustic problems, which have an unbounded acoustic domain.

In this framework, an artificial boundary surface Ω_e is introduced at some finite distance from the boundary surface Ω . Consequently, the original

* since the total number of modes equals the total number of degrees of freedom of the model, no model size reduction would then be obtained.

unbounded fluid domain V is split into a bounded domain V_1 between Ω and Ω_e and an unbounded domain V_2 between Ω_e and Ω_∞ (see Fig. 2.4).

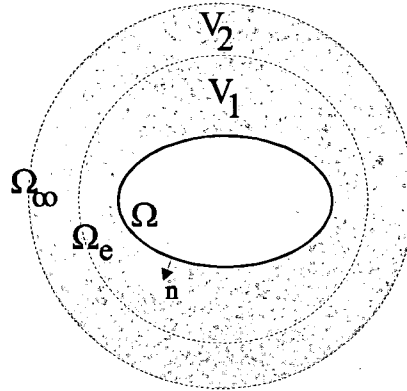


Fig. 2.4: computational domains for exterior problems

The bounded domain V_1 is suited for a finite element discretization. To get a well-posed acoustic problem in this domain, an appropriate boundary condition must be specified at the artificial boundary surface Ω_e . In this way, an exterior problem is dealt with as an approximate interior problem.

For exterior acoustic problems, the Sommerfeld radiation condition must be satisfied at the boundary surface Ω_∞ to ensure that all acoustic waves propagate freely towards infinity and that no reflections occur at this boundary,

$$\lim_{|\vec{r}| \rightarrow \infty} |\vec{r}| \left(\frac{\partial p(\vec{r})}{\partial |\vec{r}|} + jk p(\vec{r}) \right) = 0 \quad (2.66)$$

Several approaches can be used to approximate this radiation condition.

1. The simplest approach is to use the specific acoustic impedance of freely propagating plane waves as impedance boundary condition for the pressure and normal fluid velocity at the artificial boundary surface Ω_e (see e.g. [2.18]),

$$p(\mathbf{r}) = \rho_0 c v_n(\mathbf{r}), \quad \mathbf{r} \in \Omega_e \quad (2.67)$$

For this boundary condition to be (quasi) non-reflective for the acoustic waves in an exterior fluid domain, the distance between the artificial boundary surface Ω_e and the boundary surface Ω must be very large. As a result, the bounded domain V_1 is still very large, which yields a very large and computationally expensive finite element model.

2. A more advanced approach consists of using 'damping' elements at the artificial boundary surface of the finite element discretization of domain V_1 in order to approximately model the absorption of outgoing acoustic waves. This approach was initially proposed by [2.10], [2.11] and has been refined by [2.15], [2.45] and [2.2], [2.3]. A surface with a simple geometrical shape, usually a sphere, is selected as artificial boundary surface Ω_e . The pressure field in the unbounded domain V_2 is approximated in terms of an analytical multipolar expansion of outgoing wave functions that satisfy the Sommerfeld radiation condition. The evaluation of this analytical expansion at the artificial boundary surface Ω_e yields the pressure values, which are imposed at the boundary nodes of the 'damping' elements, located at the artificial boundary surface in the finite element discretization of domain V_1 . For 'monopolar damping' elements, which are based on a monopolar pressure expansion, the artificial boundary surface

must be located in the far-field of the exterior pressure at a large distance from the boundary surface Ω_e . For 'dipolar damping' elements, the extent of the domain V_1 can be quite limited and becomes attractive for finite element discretization.

3. The Dirichlet-to-Neumann method (DtN method) is based on an exact formulation of the boundary condition at the artificial boundary surface Ω_e . [2.37] proposed an analytical solution for the pressure field in the unbounded domain V_2 that satisfies the Sommerfeld radiation condition and an arbitrary Dirichlet condition (imposed pressure condition) on the artificial boundary surface. They used this solution to form a relation between the pressure and its normal gradient at the artificial boundary surface Ω_e , which yields the exact impedance boundary condition. The finite element implementation of this exact Dirichlet-to-Neumann impedance boundary condition has been discussed by [2.33], [2.48] and [2.30]. Since this method allows the artificial boundary surface Ω_e to be located in the near-field of the exterior pressure, only a small domain V_1 must be discretized, which yields a fairly small finite element model.
4. Instead of using an analytical expression for the pressure field in the unbounded domain V_2 and for the derivation of the boundary condition on the artificial boundary surface Ω_e , the pressure field in V_2 can also be approximated numerically through the use of an infinite element discretization of this unbounded domain ([2.14], [2.13], [2.1]). Each of the infinite elements in such a discretization contains a part of the artificial boundary surface Ω_e and is infinitely extended away from the artificial boundary surface. In this way, the infinite elements span as a single layer around the conventional finite elements, used for the pressure field in the domain V_1 . The pressure within the infinite elements is expressed in terms of shape functions with a built-in amplitude decay and wave-like variation to model outgoing waves. To overcome the difficulties which arise with the numerical integrations involved in the implementation of infinite elements, infinite wave envelope elements ([2.4], [2.5]) and more recently mapped infinite wave envelope elements ([2.6], [2.24], [2.7]) have been developed. They use shape functions similar to those of regular infinite elements but use the complex conjugates of the shape functions as weighting functions. This removes all wavelike terms from the element integrals and simplifies the frequency dependence of the resulting model matrices.

The size of the resulting model, consisting of a finite element model for the acoustic domain V_1 and an infinite element model for the acoustic domain V_2 , is strongly dependent on the location of the artificial boundary surface Ω_e and the subsequent size of domain V_1 . The size of domain V_1 is in its turn strongly related to the shape functions, used in the infinite elements in domain V_2 . The more accurate these shape functions can represent outwards travelling waves, the smaller the size of domain V_1 can be to get an accurate prediction of the coupled response in exterior vibro-acoustic systems. In this framework, [2.16] has proposed the use of spheroidal co-ordinate systems for the formulation of the infinite element shape functions. This permits the required extent of domain V_1 to be reduced in the case of slender objects.

2.8 Coupled vibro-acoustic problems

For coupled vibro-acoustic problems, an acoustic and a structural problem must be solved simultaneously to include the mutual coupling interaction between the fluid pressure and the structural deformation. The most commonly used technique for interior coupled problems, which have a bounded acoustic domain,

is a coupled FE/FE model, in which an acoustic FE model is coupled with a structural FE model.

2.8.1 Problem definition

In an interior coupled vibro-acoustic system, the fluid is comprised in a bounded acoustic domain V , of which the boundary surface Ω_a contains an elastic structural surface Ω_s ($\Omega_a = \Omega_s \cup \Omega_p \cup \Omega_v \cup \Omega_z$), as shown in Fig. 2.5.

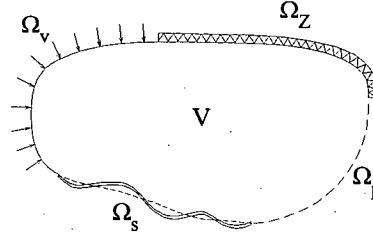


Fig. 2.5: interior coupled vibro-acoustic system

fluid pressure field

As for uncoupled acoustic problems (see section 2.2), the steady-state acoustic pressure in the fluid domain V is governed by the Helmholtz equation

$$\nabla^2 p(x, y, z) + k^2 \cdot p(x, y, z) = -j\rho_0\omega \cdot q(x, y, z) \quad (2.68)$$

For interior coupled vibro-acoustic systems, four different types of acoustic boundary conditions may be specified on the boundary surface Ω_a of domain V .

- imposed pressure :

$$p = \bar{p} \quad \text{on } \Omega_p \quad (2.69)$$

- imposed normal velocity :

$$v_n = \frac{j}{\rho_0\omega} \frac{\partial p}{\partial n} = \bar{v}_n \quad \text{on } \Omega_v \quad (2.70)$$

- imposed normal impedance :

$$p = \bar{Z} \cdot v_n = \frac{v_n}{A} = \frac{j\bar{Z}}{\rho_0\omega} \frac{\partial p}{\partial n} = \frac{j}{\rho_0\omega A} \frac{\partial p}{\partial n} \quad \text{on } \Omega_z \quad (2.71)$$

- normal velocity continuity:

$$v_n = \frac{j}{\rho_0\omega} \frac{\partial p}{\partial n} = j\omega w_n \quad \text{on } \Omega_s \quad (2.72)$$

The last boundary condition expresses the vibro-acoustic coupling condition, in that the normal fluid velocity must equal the normal structural velocity along the fluid-structure coupling interface Ω_s .

structural displacement field

Although any type of elastic structure could be part of a coupled vibro-acoustic system, the elastic structure is assumed to be a shell-type structure, which has a small thickness dimension, since significant vibro-acoustic coupling effects occur mainly for elastic structures with a small stiffness and mass.

For this type of structures, the displacement field is usually characterized in terms of the displacement components of the shell middle surface, which may be

described in a local co-ordinate system (s1,s2,n), attached to the middle surface (see Fig. 2.6). The co-ordinate directions s1 and s2 are located in the plane of the middle surface, while n represents the direction normal to the middle surface with positive orientation away from the fluid domain.

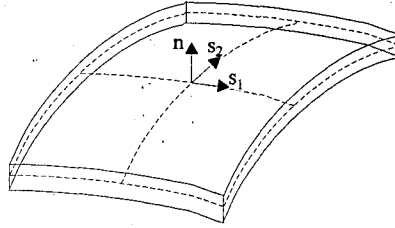


Fig. 2.6: shell co-ordinate system

The corresponding middle surface displacement components w_{s1} , w_{s2} and w_n are governed by the following type of linear dynamic equations,

$$\left[\hat{\mathbf{L}}_s \right] - \omega^2 \left[\hat{\mathbf{M}}_s \right] \cdot \begin{Bmatrix} w_{s1}(\mathbf{r}) \\ w_{s2}(\mathbf{r}) \\ w_n(\mathbf{r}) \end{Bmatrix} = \begin{Bmatrix} \tilde{f}_{s1}(\mathbf{r}) \\ \tilde{f}_{s2}(\mathbf{r}) \\ \tilde{f}_n(\mathbf{r}) \end{Bmatrix} + \begin{Bmatrix} 0 \\ 0 \\ p(\mathbf{r}) \end{Bmatrix}, \quad \mathbf{r} \in \Omega_s. \quad (2.73)$$

$\left[\hat{\mathbf{L}}_s \right]$ is a (3x3) matrix of differential operators, governing the elastic and damping forces in the shell structure and the elements of the (3x3) matrix $\left[\hat{\mathbf{M}}_s \right]$ represent the inertial parameters of the structure. The first term in the right-hand side of Eq. (2.73) represents the distribution of mechanically applied forces (force per unit area) on the structure. The second term represents the fluid pressure loading. Since the fluid has no viscosity, the fluid pressure exerts only a force excitation in the normal direction. Note that, although assumed in Eq. (2.73) for the sake of simplicity, the elastic structure needs not to be completely in contact with the fluid.

The dynamic Eq. (2.73) describe the different wavetypes in the elastic structure. With s being the number of wavetypes, the structural displacement field is uniquely defined, if s boundary conditions are specified at each point of the boundary Γ_s of surface Ω_s . A general formulation of these boundary conditions is

$$\left[\hat{\mathbf{L}}_{s,b} \right] \cdot \begin{Bmatrix} w_{s1}(\mathbf{r}) \\ w_{s2}(\mathbf{r}) \\ w_n(\mathbf{r}) \end{Bmatrix} = \{ \bar{g}_s(\mathbf{r}) \}, \quad \mathbf{r} \in \Gamma_s, \quad (2.74)$$

where $\left[\hat{\mathbf{L}}_{s,b} \right]$ is a (sx3) matrix of differential operators, governing the appropriate boundary conditions and $\{ \bar{g}_s(\mathbf{r}) \}$ is a (sx1) vector of corresponding prescribed functions.

2.8.2 Model types

The coupled FE/FE models can be classified into three major categories, based on the approach used in the problem formulation : the Eulerian, the Lagrangian and the mixed approach.

2.8.2.1 Eulerian model

In an Eulerian formulation, the acoustic response is described by a single scalar function, usually the pressure, while the structural response is described by the displacement vector.

acoustic FE model

As described in section 2.3, the finite element approximation of the steady-state pressure p in the bounded fluid domain V is an expansion \hat{p} in terms of a set of global shape functions N_i ,

$$\begin{aligned}\hat{p}(x, y, z) &= \sum_{i=1}^{n_a} N_i(x, y, z) \cdot p_i + \sum_{i=1}^{n_p} N_i(x, y, z) \cdot \bar{p}_i \\ &= [N_a] \{p_i\} + [N_p] \{\bar{p}_i\}, \quad (x, y, z) \in V,\end{aligned}\quad (2.75)$$

where n_p is the number of constrained degrees of freedom, i.e. the prescribed pressure values \bar{p}_i at the n_p nodes, which are located on the part Ω_p of the boundary surface, on which a prescribed pressure boundary condition is imposed. The global shape functions, associated with these constrained degrees of freedom, are comprised in the $(1 \times n_p)$ vector $[N_p]$. The n_a unconstrained degrees of freedom are comprised in the $(n_a \times 1)$ vector $\{p_i\}$ and their associated global shape functions are comprised in the $(1 \times n_a)$ vector $[N_a]$. The resulting finite element model for the unconstrained degrees of freedom takes the form,

$$\left([K_a] + j\omega[C_a] - \omega^2[M_a] \right) \{p_i\} = \{F_a\} \quad (2.76)$$

The $(n_a \times 1)$ vector $\{F_a\}$ contains the terms in the constrained degrees of freedom, the contributions from the external acoustic sources in the fluid domain V and the contributions from the prescribed velocity input, imposed on part Ω_v of the boundary surface (2.70). The latter contributions are expressed as (see (2.29))

$$\int_{\Omega_v} (-j\rho_0\omega [N_a]^T \bar{v}_n) \cdot d\Omega \quad (2.77)$$

where \bar{v}_n is the prescribed normal fluid velocity, with positive orientation away from the fluid domain V .

structural FE model

As described e.g. by [2.54], the finite element approximations of the steady-state dynamic displacement components of the middle surface Ω_s of an elastic shell structure in the x -, y - and z -direction of a global Cartesian co-ordinate system are

$$\begin{Bmatrix} \hat{w}_x(x, y, z) \\ \hat{w}_y(x, y, z) \\ \hat{w}_z(x, y, z) \end{Bmatrix} = [N_s] \{w_i\} + [N_w] \{\bar{w}_i\} \quad (2.78)$$

where the $(3 \times n_w)$ matrix $[N_w]$ comprises the global shape functions, which are associated with the n_w constrained degrees of freedom, i.e. the prescribed translational and rotational displacements \bar{w}_i at nodes, which are located on the part of the shell boundary, on which prescribed translational and/or rotational displacements are imposed. The n_s unconstrained translational and rotational displacement degrees of freedom are comprised in the $(n_s \times 1)$ vector $\{w_i\}$ and their associated global shape functions are comprised in the $(3 \times n_s)$ matrix $[N_s]$.

The resulting finite element model for the unconstrained degrees of freedom takes the form,

$$\left([K_s] + j\omega[C_s] - \omega^2[M_s] \right) \{w_i\} = \{F_s\} \quad (2.79)$$

The (nsxns) matrices $[K_s]$, $[M_s]$ and $[C_s]$ are the structural stiffness, mass and damping matrices. The (nsx1) vector $\{F_s\}$ contains the terms in the constrained degrees of freedom, the contributions from the prescribed forces and moments, applied on (part of) the shell boundary and the contributions from the external load p , applied normal to the shell surface Ω_s . The latter contributions are expressed as

$$\sum_{e=1}^{n_{se}} \left(\int_{\Omega_{se}} \left([N_s]^T \cdot \{n^e\} \cdot p \right) d\Omega \right) \quad (2.80)$$

where n_{se} is the number of flat plate elements Ω_{se} in the shell discretization and where the unit vector, normal to a plate element, is represented in the (3x1) vector $\{n^e\}$.

coupling of both models

The force loading of the acoustic pressure on the elastic shell structure along the fluid-structure coupling interface in an interior coupled vibro-acoustic system may be regarded as an additional normal load. As a result, an additional term of type (2.80), using the acoustic pressure approximation (2.75), must be added to the structural FE model (2.79). When it is assumed that the elastic shell structure is completely comprised in the boundary surface of the fluid domain, the structural FE model (2.79) modifies to

$$\left([K_s] + j\omega[C_s] - \omega^2[M_s] \right) \{w_i\} + [K_c] \{p_i\} = \{F_{si}\} \quad (2.81)$$

The (nsxna) coupling matrix $[K_c]$ is

$$[K_c] = - \sum_{e=1}^{n_{se}} \left(\int_{\Omega_{se}} \left([N_s]^T \cdot \{n^e\} \cdot [N_a] \right) d\Omega \right) \quad (2.82)$$

and the (nsx1) excitation vector $\{F_{si}\}$ is

$$\{F_{si}\} = \{F_s\} + \sum_{e=1}^{n_{se}} \left(\int_{\Omega_{se}} \left([N_s]^T \cdot \{n^e\} \cdot [N_p] \{ \bar{p}_i \} \right) d\Omega \right) \quad (2.83)$$

The continuity of the normal shell velocities and the normal fluid velocities at the fluid-structure coupling interface may be regarded as an additional velocity input on the part Ω_s of the boundary surface of the acoustic domain. As a result, an additional term of type (2.77), using the shell displacement approximations (2.78), must be added to the acoustic FE model (2.76). This modified acoustic FE model becomes

$$\left([K_a] + j\omega[C_a] - \omega^2[M_a] \right) \{p_i\} - \omega^2[M_c] \{w_i\} = \{F_{ai}\} \quad (2.84)$$

The (naxns) coupling matrix $[M_c]$ is

$$[M_c] = \sum_{e=1}^{n_{se}} \left(\int_{\Omega_{se}} \left(\rho_0 [N_a]^T \cdot \{n^e\}^T \cdot [N_s] \right) \cdot d\Omega \right) \quad (2.85)$$

and the (nax1) excitation vector $\{F_{ai}\}$ is

$$\{F_{ai}\} = \{F_a\} + \sum_{e=1}^{n_{se}} \left(\int_{\Omega_{se}} \rho_0 \omega^2 \left([N_a]^T \cdot \{n^e\}^T \cdot [N_w] \{w_i\} \right) \cdot d\Omega \right) \quad (2.86)$$

A comparison between the coupling matrices (2.82) and (2.85) indicates that

$$[M_c] = -\rho_0 [K_c]^T \quad (2.87)$$

Combining the modified structural FE model (2.81) and the modified acoustic FE model (2.84) yields the Eulerian FE/FE model for an interior coupled vibro-acoustic system,

$$\left(\begin{bmatrix} K_s & K_c \\ 0 & K_a \end{bmatrix} + j\omega \begin{bmatrix} C_s & 0 \\ 0 & C_a \end{bmatrix} - \omega^2 \begin{bmatrix} M_s & 0 \\ -\rho_0 K_c^T & M_a \end{bmatrix} \right) \cdot \begin{Bmatrix} w_i \\ p_i \end{Bmatrix} = \begin{Bmatrix} F_{si} \\ F_{ai} \end{Bmatrix} \quad (2.88)$$

The coefficients in the coupled stiffness matrix and coupled mass matrix are still frequency independent but, in contrast with an uncoupled structural or uncoupled acoustic finite element model, these coupled matrices are no longer symmetric. This is due to the fact that the force loading of the fluid on the structure is proportional to the pressure, resulting in a cross-coupling matrix $[K_c]$ in the coupled stiffness matrix, while the force loading of the structure on the fluid is proportional to the acceleration, resulting in a cross-coupling matrix $[-\rho_0 K_c^T]$ in the coupled mass matrix.

Note that for the practical calculation of this coupled model, it is convenient that the acoustic and structural meshes are matching, i.e. that the nodes of the acoustic and the structural meshes at the fluid-structure coupling interface coincide. If not, the structural nodal displacement degrees of freedom must be related to the acoustic nodal pressure degrees of freedom along the fluid-structure coupling interface through some geometrical transfer matrices, as proposed e.g. by [2.19].

Due to the cross-coupling matrices, the banded, sparsely populated nature of the matrices in an uncoupled finite element model partly vanishes in a coupled finite element model. As a consequence, the efficient equation solvers and eigenvalue solvers for sparse symmetric matrices can no longer be used and have to be replaced by non-symmetric solvers, which are more time expensive. For this reason, the undamped natural frequencies and mode shapes at low frequencies are often calculated by assuming an incompressible fluid ($[M_a] = [0]$), which yields a simpler eigenvalue problem,

$$\left([K_s] - \omega^2 \left([M_s] + [\tilde{M}] \right) \right) \{w_i\} = \{0\} \quad (2.89)$$

where $[\tilde{M}]$ is referred to as the added mass matrix,

$$[\tilde{M}] = \rho_0 [K_c] [K_a]^{-1} [K_c]^T \quad (2.90)$$

In an alternative Eulerian formulation ([2.27], [2.43]), the fluid is described by the fluid velocity potential φ , of which the gradient vector equals the fluid velocity vector \vec{v} ,

$$\vec{v} = \frac{j}{\rho_0 \omega} \vec{\nabla} p = \vec{\nabla} \varphi. \quad (2.91)$$

This choice renders the symmetric model,

$$\begin{aligned} & \left(\begin{bmatrix} K_s & 0 \\ 0 & -\rho_0 K_a \end{bmatrix} + j\omega \begin{bmatrix} C_s & -\rho_0 K_c \\ -\rho_0 K_c^T & -\rho_0 C_a \end{bmatrix} - \omega^2 \begin{bmatrix} M_s & 0 \\ 0 & -\rho_0 M_a \end{bmatrix} \right) \begin{Bmatrix} w_i \\ \varphi_i \end{Bmatrix} \\ & = \begin{Bmatrix} F_{si} \\ F_{ai} \\ j\omega \end{Bmatrix} \end{aligned} \quad (2.92)$$

For damped systems, this symmetric formulation is obtained without any penalty. For undamped systems ($[C_s] = [C_a] = [0]$), the use of the fluid velocity potential yields a symmetric model, which becomes, however, complex due to the introduction of an artificial damping matrix. This is disadvantageous in terms of computational effort since solving a non-symmetric but real model, obtained from an undamped pressure formulation (see (2.88)), requires less arithmetical operations than solving a symmetric but complex model, obtained from a velocity potential formulation (see (2.92)).

2.8.2.2 Lagrangian model

In a Lagrangian formulation, both structural and acoustic responses are described by their displacement vector ([2.28]). Since both the force loading of the structure on the fluid as well as the force loading of the fluid on the structure are proportional to the structural/fluid acceleration, the coupled system matrices in a Lagrangian formulation are symmetric. However, the advantage of symmetry can hardly counterbalance the drawbacks of the formulation.

A first drawback is the substantial increase of the size of the coupled problem, since the fluid displacement has three vector components instead of one scalar value (pressure or fluid velocity potential) for each node of the acoustic mesh.

A second, and more severe, drawback is the existence of spurious rotational modes. Under the assumption of an inviscid fluid, the shear modulus of the fluid is zero and hence, the fluid motion is irrotational. The Lagrangian formulation results from the application of the variational principle to an energy functional. Since the shear modulus of an inviscid fluid is zero, the matrix D , linking the fluid stresses to the fluid strains ($\sigma = D \cdot \epsilon$), is singular. This allows zero-energy rotational deformation modes, which are not excluded from the Lagrangian model since these spurious modes don't contribute to the energy functional. In order to avoid these physically unfeasible modes, an additional irrotationality constraint of the fluid has to be imposed by a penalty method ([2.32], [2.53], [2.12], [2.42]). This is done by adding an additional rotational energy functional $J^{(r)}$, weighted by a penalty factor α , to the energy functional,

$$\alpha \cdot J^{(r)}(\vec{u}) = \frac{1}{2} \alpha \cdot \int_{V_a} (\vec{\nabla} \times \vec{u})^2 dV_a \quad (2.93)$$

where V_a is the acoustic domain and $\vec{u} (= \vec{v} / (j\omega))$ is the fluid displacement vector. The resulting system equations are, in absence of any type of damping,

$$\left([L]^T \begin{bmatrix} \tilde{K}_s & 0 \\ 0 & \tilde{K}_a + \alpha \tilde{K}_a \end{bmatrix} [L] - \omega^2 (\alpha) [L]^T \begin{bmatrix} \tilde{M}_s & 0 \\ 0 & \tilde{M}_a \end{bmatrix} [L] \right) \{ \tilde{V}_i \} = \begin{Bmatrix} \tilde{F}_s \\ \tilde{F}_a \end{Bmatrix} \quad (2.94)$$

with $\begin{Bmatrix} w_i \\ u_i \end{Bmatrix} = [L] \{ V_i \}$.

Based on the coupling conditions at the fluid-structure interface, matrix $[L]$ represents the static condensation of all nodal structural displacement components w_i and nodal fluid displacement components u_i in terms of the displacements V_i at the nodes which do not belong to the fluid-structure interface. $[\tilde{K}_s]$ and $[\tilde{K}_a]$, $[\tilde{M}_s]$ and $[\tilde{M}_a]$ are the structural and acoustic stiffness and mass matrices. Matrix $[\tilde{K}_a]$ results from the irrotationality constraint. $\{\tilde{F}_s\}$ and $\{\tilde{F}_a\}$ are the external nodal structural and acoustic excitation vectors. Only a penalty factor $\alpha = \alpha$ ensures an irrotational acoustic response. Since the system equations can only be solved for a finite value of α , the response vectors and eigensolutions depend on α and satisfy the irrotationality constraint only in an approximate way.

To remove the deficiency of spurious rotational modes, [2.9] have proposed an advanced Lagrangian formulation, using the displacement, pressure and a 'vorticity moment' as acoustic variables. The two latter variables are associated with element internal variables and are statically condensed out at element level, so that only the nodal fluid displacements occur in the global coupled model.

2.8.2.3 Mixed model

In mixed formulations, the structural response is described by its displacement vector and the acoustic response is described by the pressure and the fluid displacement potential ψ , whose gradient is proportional to the fluid displacement. The fluid-structure coupling interaction can be introduced as cross-coupling matrices in the coupled mass matrix ([2.39]). A more advantageous mixed formulation introduces the fluid-structure coupling interaction as cross-coupling matrices in the coupled stiffness matrix ([2.41], [2.46]). In absence of any type of damping, the latter formulation is

$$\left(\begin{bmatrix} K_s & 0 & -M_c^T \\ 0 & 0 & B_a^T \\ -M_c & B_a & -M_a \end{bmatrix} - \omega^2 \begin{bmatrix} M_s & 0 & 0 \\ 0 & K_a & 0 \\ 0 & 0 & 0 \end{bmatrix} \right) \begin{Bmatrix} w_i \\ \psi_i \\ p_i \end{Bmatrix} = \begin{Bmatrix} F_{si} \\ 0 \\ F_{ai} \end{Bmatrix} \quad (2.95)$$

$[M_c]$ results from the fluid-structure coupling interaction and $[B_a]$ relates the nodal fluid pressures to the nodal fluid displacement potentials.

The system equations are symmetric, no third artificial damping matrix is introduced and no spurious rotational modes are present.

This mixed formulation has, however, two major drawbacks. First of all, the size of the coupled problem is substantially larger, compared to the Eulerian formulation (2.88), since there are two degrees of freedom for each acoustic node. Secondly, special equation and eigenvalue solvers are required, since the coupled stiffness matrix is indefinite and the coupled mass matrix is positive semi-definite.

At present, a comparison of the advantages and drawbacks of the different symmetric formulations with those of the non-symmetric Eulerian pressure formulation (2.88) denotes the latter as the most appropriate prediction

technique. Therefore, most of the available finite elements programs (e.g. SYSNOISE, MSC/NASTRAN, ANSYS) use the Eulerian pressure formulation for coupled predictions of interior coupled vibro-acoustic systems.

2.8.3 Model size reduction techniques

For the uncoupled structural and uncoupled acoustic problems, encountered in uncoupled vibro-acoustic systems, their model sizes and subsequent computational efforts may be efficiently reduced by using model size reduction techniques, such as the modal expansion technique, the component mode synthesis and the Ritz vector expansion technique. For coupled vibro-acoustic problems, however, the efficiency of these model size reduction techniques is significantly reduced, as discussed below.

2.8.3.1 Modal expansion

In the *modal expansion technique*, the dynamic field variables are expanded in terms of the modes of the considered system (cf. section 2.6.2.). For element based models, the contributions of the different modes to the dynamic response become the unknowns of the modal model instead of the nodal degrees of freedom in the original model. Although all modes should be used to get the same accuracy as with the original model*, a relatively small truncated set of modes yields already a level of accuracy close to the one of the much larger original model. In this framework, a rule of thumb states that an accurate prediction of the steady-state dynamic behavior in a certain frequency range is obtained by using all modes with natural frequencies, smaller than twice the upper frequency limit of the considered frequency range. Especially in the low-frequency range, where modal densities are small, this yields a significant model size reduction.

In addition to the reduced model size, the matrices in a modal model often become diagonal due to the orthogonality properties of the modes. As a result, when the steady-state response is needed at a large number of frequencies, the computational effort for constructing the modal base and then solving the reduced modal model at each frequency of interest is usually substantially smaller than for directly solving the original model at each frequency.

The modal expansion technique for coupled Eulerian models (2.88) is applied as follows.

The predictions for the undamped mode shapes and natural frequencies of a coupled vibro-acoustic system result from the following right eigenvalue problem,

$$\begin{bmatrix} K_s & K_c \\ 0 & \frac{1}{\rho_0} K_a \end{bmatrix} \{\Phi_c\} = \omega_c^2 \begin{bmatrix} M_s & 0 \\ -K_c^T & \frac{1}{\rho_0} M_a \end{bmatrix} \{\Phi_c\} \quad (c = 1..n_s + n_a) \quad (2.96)$$

where each $((n_s+n_a) \times 1)$ right eigenvector $\{\Phi_c\}$ represents a mode shape and where the associated eigenvalue corresponds with the squared value of the natural frequency ω_c of that mode.

Since, in contrast with uncoupled acoustic and uncoupled structural FE models, the stiffness and mass matrices in a coupled Eulerian model are no longer symmetric, the above eigenvalue problem is non-symmetric. Hence, the left eigenvectors $\{\bar{\Phi}_c\}$ of the associated left eigenvalue problem,

* since the total number of modes equals the total number of degrees of freedom of the model, no model size reduction would be obtained

$$\{\bar{\Phi}_c\}^T \begin{bmatrix} K_s & K_c \\ 0 & \frac{1}{\rho_0} K_a \end{bmatrix} = \omega_c^2 \{\bar{\Phi}_c\}^T \begin{bmatrix} M_s & 0 \\ -K_c^T & \frac{1}{\rho_0} M_a \end{bmatrix} \quad (2.97)$$

differ from the right eigenvectors $\{\Phi_c\}$. However, [2.38] indicated that, due to the particular matrix relation (2.87), the components, which correspond with the n_a acoustic degrees of freedom in each pair of associated left and right eigenvectors, are identical and that the components, which correspond with the n_s structural degrees of freedom in the left eigenvectors, are proportional to the corresponding right eigenvector components with a factor, equal to the associated eigenvalue,

$$\{\bar{\Phi}_c\} = \begin{Bmatrix} \bar{\Phi}_{sc} \\ \bar{\Phi}_{ac} \end{Bmatrix} = \begin{Bmatrix} \omega_c^2 \Phi_{sc} \\ \Phi_{ac} \end{Bmatrix} \quad (c = 1, n_s + n_a) \quad (2.98)$$

The Eulerian model (2.88) may be transformed into a modal model by expanding the nodal degrees of freedom in terms of a set of $m_c (\leq n_s + n_a)$ modes of the coupled vibro-acoustic system,

$$\begin{Bmatrix} w_i \\ p_i \end{Bmatrix} = \sum_{c=1}^{m_c} \phi_c \begin{Bmatrix} \Phi_{sc} \\ \Phi_{ac} \end{Bmatrix} = [\Phi] \{\phi_c\} \quad (2.99)$$

where $[\Phi]$ is a $((n_s + n_a) \times m_c)$ matrix of right eigenvectors and where $\{\phi_c\}$ is a $(m_c \times 1)$ vector of modal participation factors.

By substituting the modal expansion (2.99) into the Eulerian model (2.88), in which all equations of the acoustic part are divided by ρ_0 , and by premultiplying both sides of the resulting matrix equation with the transpose of the $((n_s + n_a) \times m_c)$ matrix of corresponding left eigenvectors, the following modal model is obtained,

$$([\tilde{K}] + j\omega[\tilde{C}] - \omega^2[\tilde{M}])\{\phi_c\} = \{\tilde{F}\} \quad (2.100)$$

where the $(m_c \times 1)$ modal excitation vector is

$$\{\tilde{F}\} = [\bar{\Phi}]^T \begin{Bmatrix} F_{si} \\ \frac{1}{\rho_0} F_{ai} \end{Bmatrix} \quad (2.101)$$

and where the $(m_c \times m_c)$ modal stiffness, mass and damping matrices are

$$[\tilde{K}] = [\bar{\Phi}]^T \begin{bmatrix} K_s & K_c \\ 0 & \frac{1}{\rho_0} K_a \end{bmatrix} [\Phi], \quad [\tilde{M}] = [\bar{\Phi}]^T \begin{bmatrix} M_s & 0 \\ -K_c^T & \frac{1}{\rho_0} M_a \end{bmatrix} [\Phi], \quad (2.102)$$

$$[\tilde{C}] = [\bar{\Phi}]^T \begin{bmatrix} C_s & 0 \\ 0 & \frac{1}{\rho_0} C_a \end{bmatrix} [\Phi].$$

Due to the orthogonality of the left and right eigenvectors with respect to the mass matrix,

$$\{\bar{\Phi}_{c_1}\}^T \begin{bmatrix} M_s & 0 \\ -K_c^T & \frac{1}{\rho_0} M_a \end{bmatrix} \{\Phi_{c_2}\} = 0, \quad \text{if } c_1 \neq c_2, \quad (2.103)$$

the modal mass and modal stiffness matrices are diagonal matrices. By normalizing the eigenvectors, according to

$$\{\bar{\Phi}_{c_l}\}^T \begin{bmatrix} M_s & 0 \\ -K_c^T & \frac{1}{\rho_0} M_a \end{bmatrix} \{\Phi_{c_l}\} = 0, \quad (c_l = 1..m_c), \quad (2.104)$$

the modal mass matrix becomes the unity matrix,

$$[\tilde{M}] = \begin{bmatrix} 1 & & \\ & \ddots & \\ & & 1 \end{bmatrix} \quad (2.105)$$

and the diagonal modal stiffness matrix becomes

$$[\tilde{K}] = \begin{bmatrix} \omega_1^2 & & \\ & \ddots & \\ & & \omega_{m_c}^2 \end{bmatrix} \quad (2.106)$$

The fact that the left and right eigenvector result from a non-symmetric eigenvalue problem, puts, however, a severe practical limitation on the use of the modal expansion technique for coupled vibro-acoustic problems.

In contrast with the symmetric eigenvalue problems for uncoupled structural and uncoupled acoustic models, the non-symmetric eigenvalue problems for coupled models are much more computationally demanding.

To illustrate this, a rectangular acoustic cavity with a length of 1 m, a width of 0.5 m and a height of 0.15 m is considered. One side of the cavity consists of a flexible, rectangular plate of 1 m x 0.5 m with clamped boundaries, while the five other cavity side walls are perfectly rigid. Three structural discretizations are built with 4-noded rectangular plate elements (CQUAD4), six acoustic discretizations are built with 8-noded rectangular fluid elements (CHEXA8), yielding six discretizations for the coupled system. Tab. 2.1 lists the number of elements in the structural and acoustic discretizations and the resulting numbers n_s , n_a and n_c of unconstrained degrees of freedom of the different FE models.

structural		acoustic		coupled
$n_x \times n_y$	n_s	$n_x \times n_y \times n_z$	n_a	$n_c = n_s + n_a$
20x12	627	20x12x4	1365	1992
		20x12x8	2457	3084
40x24	2691	40x24x4	5125	7816
		40x24x8	9225	11916
60x36	6195	60x36x4	11285	17480
		60x36x8	20313	26508

Tab. 2.1: numbers n_s, n_a, n_c of unconstrained degrees of freedom (n_x, n_y, n_z : number of elements in the length, width and height of the acoustic cavity)

The first 10 modes of the considered finite elements models have been calculated with the MSC/NASTRAN software on a Hewlett-Packard-C180 workstation (SPECfp95=18.7, SPECint95=11.8). The involved CPU-times are plotted against the corresponding number of unconstrained degrees of freedom in Fig. 2.7.

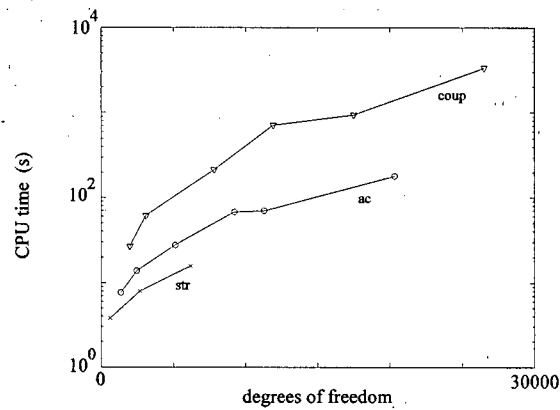


Fig. 2.7: CPU time for mode extraction from the uncoupled structural (\times), uncoupled acoustic (o) and coupled vibro-acoustic (∇) models

This figure clearly illustrates that a non-symmetric eigenvalue problem, involved with the mode extraction from coupled Eulerian FE/FE models, requires a substantially larger amount of computational effort than the symmetric eigenvalue problems, involved with the mode extraction from uncoupled structural and uncoupled acoustic FE models. Note also that the difference between the CPU times for the uncoupled structural and uncoupled acoustic models illustrates that the computational effort is not only determined by the model size, but also by the bandwidth of the sparsely populated stiffness and mass matrices.

In this way, the mode extraction becomes a computationally very expensive calculation for many coupled vibro-acoustic problems.

2.8.3.2 Component mode synthesis

Due to the problems, involved with the calculation of the modes of a coupled vibro-acoustic system, the *component mode synthesis technique* provides an alternative approach to get a model size reduction.

In this technique, a system is regarded as an assembly of several components and the dynamic variables of the total system are expanded in terms of the modes of the different system components, which can be calculated in a more efficient way than the modes of the total system. Since the system is divided into several components, some additional constraints must be specified at the interfaces between the components to enable the calculation of the component modes. This has an important influence on the resulting accuracy and efficiency of this model size reduction technique. For a detailed discussion of this technique, the reader is referred to e.g. [2.22] and [2.34].

Coupled vibro-acoustic systems are often decomposed into two components, i.e. the elastic shell structure and the acoustic fluid domain. Several types of interface boundary conditions between the structural and acoustic component may be used to determine the component modes. The most commonly used interface conditions for coupled vibro-acoustic systems are discussed below.

- [2.50] proposed the expansion of the structural nodal degrees of freedom in terms of a set of m_s modes of the uncoupled structural system, i.e. the modes of the elastic shell structure without acoustic pressure loading along the fluid-structure coupling interface, and expanding the acoustic nodal degrees of freedom in terms of a set of m_a modes of the uncoupled acoustic system, i.e. the

modes of the fluid domain with the fluid-structure coupling interface assumed to be perfectly rigid.

The application of this type of component mode synthesis technique for a coupled Eulerian model (2.88) is as follows.

The structural expansion becomes

$$\{w_i\} = \sum_{m=1}^{m_s} \phi_{sm} \cdot \{\Phi_{su,m}\} = [\Phi_{su}] \{\phi_s\} \quad (2.107)$$

where each column in the $(n_s \times m_s)$ matrix $[\Phi_{su}]$ is a modal vector $\{\Phi_{su,m}\}$ of the uncoupled elastic shell structure with natural frequency $\omega_{s,m}$,

$$[K_s] \{\Phi_{su,m}\} = \omega_{s,m}^2 [M_s] \{\Phi_{su,m}\} \quad (m = 1..m_s) \quad (2.108)$$

and where $\{\phi_s\}$ is a $(m_s \times 1)$ vector of structural modal participation factors.

The acoustic expansion is

$$\{p_i\} = \sum_{m=1}^{m_a} \phi_{am} \cdot \{\Phi_{au,m}\} = [\Phi_{au}] \{\phi_a\} \quad (2.109)$$

where each column in the $(n_a \times m_a)$ matrix $[\Phi_{au}]$ is a modal vector $\{\Phi_{au,m}\}$ of the uncoupled fluid domain with natural frequency $\omega_{a,m}$,

$$[K_a] \{\Phi_{au,m}\} = \omega_{a,m}^2 [M_a] \{\Phi_{au,m}\} \quad (m = 1..m_a) \quad (2.110)$$

and where $\{\phi_a\}$ is a $(m_a \times 1)$ vector of acoustic modal participation factors.

By substituting the component mode expansions (2.107) and (2.109), in which the uncoupled structural and acoustic modal vectors are normalized with respect to their corresponding mass matrices, into the Eulerian model (2.88) and by premultiplying the structural and acoustic part of the resulting matrix equation with the transpose of, respectively, the structural and the acoustic modal vector matrix, the following modal model is obtained,

$$\left([\hat{K}] + j\omega[\hat{C}] - \omega^2[\hat{M}] \right) \begin{Bmatrix} \phi_s \\ \phi_a \end{Bmatrix} = \{\hat{F}\} \quad (2.111)$$

The $((m_s+m_a) \times 1)$ right-hand side vector is

$$\{\hat{F}\} = \begin{bmatrix} \Phi_{su}^T & 0 \\ 0 & \Phi_{au}^T \end{bmatrix} \begin{Bmatrix} F_{si} \\ F_{ai} \end{Bmatrix} \quad (2.112)$$

The $((m_s+m_a) \times (m_s+m_a))$ modal stiffness matrix is

$$[\hat{K}] = \begin{bmatrix} \Lambda_s & A \\ 0 & \Lambda_a \end{bmatrix} \quad (2.113)$$

where the $(m_s \times m_s)$ matrix $[\Lambda_s]$ and the $(m_a \times m_a)$ matrix $[\Lambda_a]$ are diagonal matrices,

$$[\Lambda_s] = \begin{bmatrix} \omega_{s,1}^2 & & 0 \\ & \ddots & \\ 0 & & \omega_{s,m_s}^2 \end{bmatrix}, \quad [\Lambda_a] = \begin{bmatrix} \omega_{a,1}^2 & & 0 \\ & \ddots & \\ 0 & & \omega_{a,m_a}^2 \end{bmatrix}, \quad (2.114)$$

and where the $(m_s \times m_a)$ matrix $[A]$ is

$$[A] = [\Phi_{su}]^T \cdot [K_c] \cdot [\Phi_{au}] \quad (2.115)$$

The $((m_s+m_a) \times (m_s+m_a))$ modal mass matrix is

$$[\tilde{M}] = \begin{bmatrix} I_s & 0 \\ -\rho_0 A^T & I_a \end{bmatrix} \quad (2.116)$$

where $[I_s]$ and $[I_a]$ are, respectively, the $(m_s \times m_s)$ and $(m_a \times m_a)$ unity matrices.

The $((m_s+m_a) \times (m_s+m_a))$ modal damping matrix is

$$[\tilde{C}] = \begin{bmatrix} \Phi_{su}^T \cdot C_s \cdot \Phi_{su} & 0 \\ 0 & \Phi_{au}^T \cdot C_a \cdot \Phi_{au} \end{bmatrix} \quad (2.117)$$

The application of the component mode synthesis technique, using these uncoupled component modes, for a coupled Eulerian model of type (2.92) is described in e.g. [2.25] and its application for a coupled mixed model (2.95) is described in e.g. [2.31].

In comparison with the modal expansion, discussed in section 2.8.3.1., the calculation of the modal vectors are much less computationally demanding, since the modes of the uncoupled structural and uncoupled acoustic systems result from symmetric eigenvalue problems.

However, the efficiency of this component mode synthesis in reducing the size of the original (Eulerian) model is substantially smaller. This is mainly due to the inefficient way, in which the displacement continuity (2.72) at the fluid-structure coupling interface is approximated by the uncoupled acoustic modes. Since the uncoupled acoustic modes are calculated with rigid wall boundary conditions at the fluid-structure interface, the fluid displacement, normal to this interface, is zero in each mode. In this way, any combination of the uncoupled acoustic modes yields a zero normal fluid displacement and violates the displacement continuity condition. To get an accurate approximation of the near-field pressure effects in the vicinity of the fluid-structure coupling interface, which are usually associated with the displacement continuity, a lot of high-order acoustic modes should be comprised in the uncoupled modal base, which results in a large size of the modal model. Consequently, the benefit of a computationally efficient construction of the modal base is reduced by the smaller model size reduction, obtained with uncoupled component modes.

- To enhance the ability of the acoustic component modes to represent the displacement continuity and the associated near-field effects, [2.51] recently proposed to calculate the acoustic component modes with an impedance boundary condition at the fluid-structure coupling interface. Since the efficiency of this type of component mode synthesis is largely dependent on the applied impedance value, this approach is still subject of on-going research, mainly looking for a systematic procedure to determine a proper impedance value.
- Another way to enhance the accuracy of a component mode synthesis has been described by [2.26], who extended the fixed-interface component mode synthesis technique, developed by [2.23] and [2.47] for large structural problems, to coupled vibro-acoustic problems.

In this approach, the structural displacement is still expanded in terms of a set of uncoupled structural modes. The fluid pressure is expanded in terms of a set of fixed-interface modes and constraint modes. Fixed-interface modes are acoustic modes with zero pressure boundary conditions at the fluid-structure coupling interface. In each of the constraint modes, which are usually determined with a static condensation technique, one of the previously fixed interface degrees

of freedom is released. In this way, each constraint mode represents the static pressure field with a unit pressure at the released interface degree of freedom. [2.36] refined the method by determining the constraint modes with a dynamic calculation procedure. Since a large number of constraint modes are needed to get an acceptable level of accuracy, the resulting reduction of the model size and the computational effort is fairly small, which makes this approach of minor practical use for coupled vibro-acoustic problems.

2.8.3.3 Ritz vector expansion

The *Ritz vector expansion technique* provides a way to circumvent the problems, associated with the fact that the modes of a system or its components are independent of the external excitations of the system. Especially for local excitations, such as structural point forces and acoustic point sources, the forced responses often peak in the vicinity of the excitation point and attenuate rapidly away from the excitation. In order to accurately represent these local spatial patterns with excitation independent modes, a lot of high-order modes should be taken into account in the modal base of a modal expansion or component mode synthesis model. This has a disadvantageous effect on the model size and subsequent computational effort.

The Ritz vectors constitute an orthogonal set of functions, which not only depend on the dynamic properties of the system but also on the external excitations. [2.17], for instance, proposed the use of Ritz vectors for the expansion of the structural displacement and the fluid pressure in a coupled Eulerian FE/FE model (2.88). In comparison with a modal expansion model, a smaller number of Ritz vectors is needed to get an acceptable level of accuracy, since the Ritz vectors depend also on the external excitations. A Ritz vector expansion is, however, not commonly preferred to a modal expansion, since the benefit of the smaller model size is often nullified by the increased computational effort for calculating an orthogonal set of Ritz vectors.

2.8.4 Limitations of coupled FE/FE models

In comparison with uncoupled vibro-acoustic problems, the practical use of existing numerical prediction tools for coupled vibro-acoustic problems is more limited, since the involved model sizes and the associated computational efforts and memory requirements are larger and since the commonly used model size reduction techniques are less efficient.

larger model sizes

The discussion of the finite element method has already revealed the necessity of using a large number of degrees of freedom to get an acceptable level of accuracy. In comparison with uncoupled vibro-acoustic problems, the involved model sizes and the associated computational efforts and memory requirements are substantially larger for coupled vibro-acoustic problems. This is mainly due to the following reasons.

- In order to incorporate the vibro-acoustic coupling effects, the structural and the acoustic problem must be solved simultaneously, whereas for uncoupled vibro-acoustic systems, the structural and the acoustic problem may be solved in a sequential procedure.
- Coupled models are not only larger, but their numerical solution algorithms have also a smaller computational efficiency. Compared with an uncoupled structural or an uncoupled acoustic finite element model of the same size, solving a coupled Eulerian FE/FE model is computationally less efficient, since such a

coupled model is no longer symmetric and since its bandwidth is substantially larger (see (2.88)).

reduced efficiency of model size reduction techniques

For the uncoupled structural and uncoupled acoustic problems, encountered in uncoupled vibro-acoustic systems, their model sizes and subsequent computational efforts may be efficiently reduced by using model size reduction techniques, such as the modal expansion technique, the component mode synthesis and the Ritz vector expansion technique. For coupled vibro-acoustic problems, however, the efficiency of these model size reduction techniques is significantly reduced, as already discussed in section 2.8.3.

limited applicability

As already mentioned before, the number of elements in a finite element discretization should increase as the frequency increases. An increase of the number of elements yields a larger model size and requires a larger amount of computational effort and memory resources. As a result, the applicability of the finite element and boundary element method is practically restricted to a limited frequency range. Above a certain frequency limit, which depends on the nature of the problem and on the available computer resources, these prediction methods would require a prohibitively large amount of computational effort and memory resources to get an acceptable level of accuracy.

As discussed above, the model sizes and subsequent computational efforts are larger and the efficiency of model size reduction techniques is smaller for coupled vibro-acoustic problems than for uncoupled structural and uncoupled acoustic problems. For these reasons, the practical frequency upper limit for applying element based prediction techniques for coupled problems is substantially smaller than for uncoupled problems.

2.9 Examples

In this section, several properties of the finite element method are illustrated through a one-dimensional uncoupled acoustic problem and a one-dimensional coupled vibro-acoustic problem.

2.9.1 Uncoupled acoustic problem

2.9.1.1 Problem definition

A tube of length L_x is filled with a fluid with density ρ_0 and speed of sound c . At one end of the tube, a time-harmonic velocity with amplitude V (displacement amplitude X) and frequency ω is imposed, while the other end of the tube is rigid walled (see Fig. 2.8(a)).

The steady-state pressure response in the fluid is approximated using a finite element discretization, which consists of n two-noded elements of length $L=L_x/n$, yielding a total of $(n+1)$ nodes (see Fig. 2.8(b)).

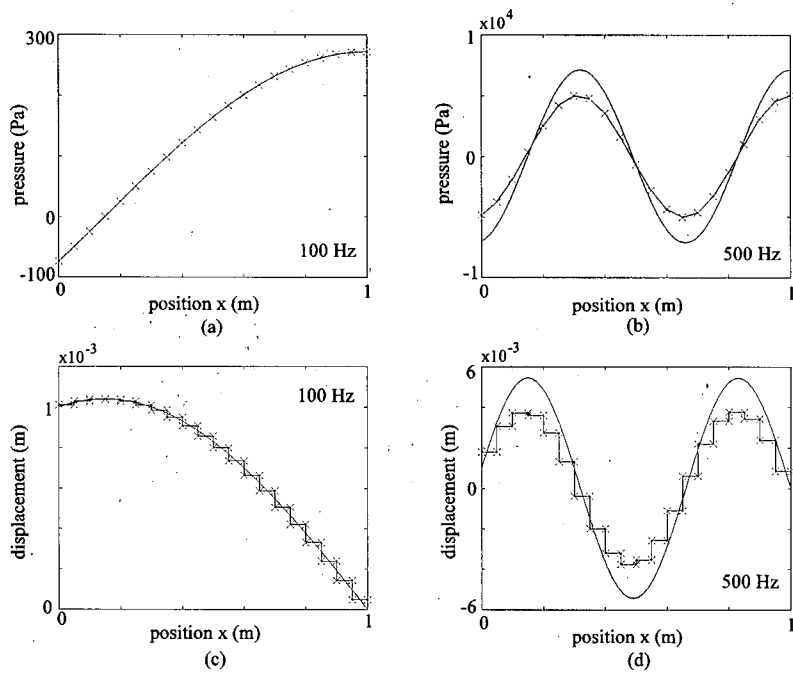


Fig. 2.9 : instantaneous steady-state pressure and displacement (solid : exact, x-marked : FE (n=20))

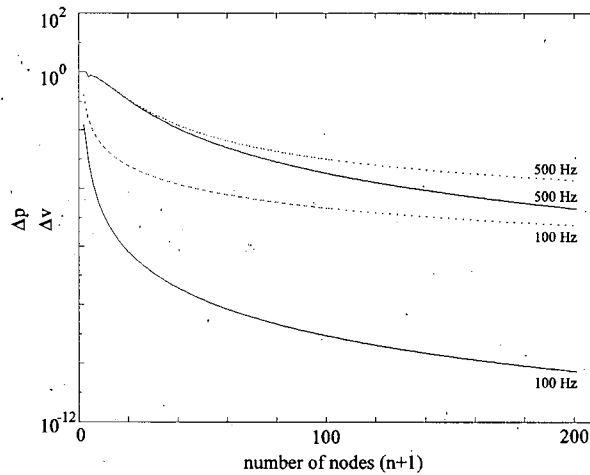


Fig. 2.10 : pressure (solid) and velocity (dotted) convergence rates

Fig. 2.9 and Fig. 2.10 illustrate some important features of the finite element prediction for solving steady-state dynamic problems.

- The accuracy, obtained from a given finite element discretization, decreases, when the excitation frequency increases

The dynamic response of an acoustic system results from a complex wave propagation mechanism in the fluid. The wavelength λ of a freely propagating

harmonic wave in a fluid is proportional to the speed of sound c in the fluid and inversely proportional to the frequency ω ,

$$\lambda = \frac{2\pi c}{\omega} \quad (2.125)$$

Consequently, the spatial variation of the dynamic response, which is strongly related to the wavelength λ , increases for increasing frequency. This is clearly illustrated in Fig. 2.9, where the period of the exact pressure oscillations in the tube corresponds with the fact that $L_x \approx 0.3\lambda$ at 100 Hz and $L_x \approx 1.5\lambda$ at 500 Hz.

Since the pressure distribution is determined by low-order polynomial shape functions, a finite element discretization yields only an approximation with a limited spatial variation. As mentioned before, a rule of thumb states that a discretization should have at least 10 elements per wavelength to keep the discretization error within acceptable limits. Hence, according to (2.125), the accuracy, obtained from a given discretization (i.e. a given number of nodes and elements), decreases with increasing frequency, as illustrated in Fig. 2.10.

- The accuracy for derived secondary variables is smaller than for primary field variables

Since the fluid velocity and displacement in a freely propagating harmonic wave have the same spatial period as the pressure, the dynamic pressure and velocity (and displacement) distributions in an acoustic system have similar spatial variations, as may be seen from the exact solutions in Fig. 2.9.

As mentioned before, the fluid velocity and displacement distributions in a finite element approximation are derived secondary variables, in that they are expressed in terms of the first-order derivatives of the pressure shape functions. Since the order of the derived velocity shape functions is smaller than the order of the pressure shape functions, the velocity and displacement approximations have a smaller spatial variation than the pressure approximation. Since this is in contrast with the above mentioned physical reality, the accuracy for the derived secondary variables in a given discretization is smaller than for the primary variables.

In the present example, in which the pressure is approximated as a linear function within each element, the corresponding velocity and displacement predictions are constant within each element and discontinuous at the element boundaries, as shown in Fig. 2.9. The subsequent accuracy of the velocity predictions in a given discretization is smaller than the pressure accuracy, as illustrated by the pressure and velocity convergence rates in Fig. 2.10.

2.9.1.3 Modal finite element model

The exact natural frequencies of the modes of the considered acoustic tube, assuming both tube ends to be perfectly rigid, are

$$f_{m,exact} = \frac{\omega_m}{2\pi} = \frac{(m-1)c}{2L_x} \quad (m = 1, 2, \dots) \quad (2.126)$$

The predictions of the modes and their natural frequencies for the finite element model (2.121), which results from a discretization of the tube into n linear elements, are obtained from the eigenvalue problem

$$[K_a]\{\Phi_m\} = \omega_m^2 [M_a]\{\Phi_m\} \quad (m = 1..(n+1)) \quad (2.127)$$

where each $((n+1) \times 1)$ eigenvector represents a predicted mode shape

$$\{\Phi_m\} = \begin{Bmatrix} p_{1,m} \\ p_{2,m} \\ \vdots \\ p_{n+1,m} \end{Bmatrix} \quad (2.128)$$

and where its associated eigenvalue represents the squared value of the predicted natural frequency.

Tab. 2.2 compares the exact and predicted natural frequencies of the first 10 modes of an air-filled ($\rho_0=1.225 \text{ kg/m}^3$, $c=340 \text{ m/s}$) tube of length $L_x=1 \text{ m}$, which is discretized into $n=100$ linear elements.

exact (126)	FE (n=100)
0 Hz	0.000 Hz
170 Hz	170.007 Hz
340 Hz	340.056 Hz
510 Hz	510.189 Hz
680 Hz	680.448 Hz
850 Hz	850.874 Hz
1020 Hz	1021.511 Hz
1190 Hz	1192.399 Hz
1360 Hz	1363.582 Hz
1530 Hz	1535.101 Hz

Tab. 2.2: exact and predicted natural frequencies

This table illustrates the typical feature of a finite element model regarding mode extraction: due to the element discretization, the natural frequencies are systematically overestimated and the absolute and relative overestimations increase for increasing frequency.

By expressing the unknown nodal pressure degrees of freedom in the finite element model (2.121) in terms of a set of m_a modal vectors, as proposed in Eq. (2.54), the modal model (2.55) for the considered acoustic tube becomes

$$\begin{bmatrix} \omega_1^2 - \omega^2 & & 0 \\ & \ddots & \\ 0 & & \omega_{m_a}^2 - \omega^2 \end{bmatrix} \begin{Bmatrix} \phi_1 \\ \vdots \\ \phi_{m_a} \end{Bmatrix} = \begin{Bmatrix} -\rho_0 \omega^2 X \cdot p_{1,1} \\ \vdots \\ -\rho_0 \omega^2 X \cdot p_{1,m_a} \end{Bmatrix} \quad (2.129)$$

where the unknowns are the modal participation factors ϕ_m in the modal expansion (2.54).

The modal model (2.129) was solved for the case of an air-filled ($\rho_0=1.225 \text{ kg/m}^3$, $c=340 \text{ m/s}$) tube of length $L_x=1 \text{ m}$ with an imposed displacement at the left hand side with amplitude $X=10^{-3} \text{ m}$ and frequency $\omega/2\pi=500 \text{ Hz}$. The tube discretization consisted of $n=100$ linear elements. Fig. 2.11 plots the resulting accuracies of the pressure and velocity predictions, indicated by their measures Δp and Δv (see (2.124)), against the number of modes m_a in the modal model.

This figure clearly indicates the efficiency of the modal expansion technique. The steep decrease of the error curves for small values of m_a indicates that a modal model with a relatively small number of modes yields an accuracy, close to the accuracy, obtained with a direct solution of the much larger finite element model. Note that the latter accuracy corresponds with a modal solution, in which all modes are taken into account ($m_a=n+1$).

As mentioned in section 2.6.2, a rule of thumb states that a good accuracy is obtained by using all the modes, whose natural frequencies are smaller than 2ω . According to this rule of thumb and to Tab. 2.2, a modal solution with the first 7

modes should have an accuracy, close to one of the direct solution, for an excitation frequency of 500 Hz. This is indeed confirmed by Fig. 2.11, in which the error measures for this modal model are '+'-marked.

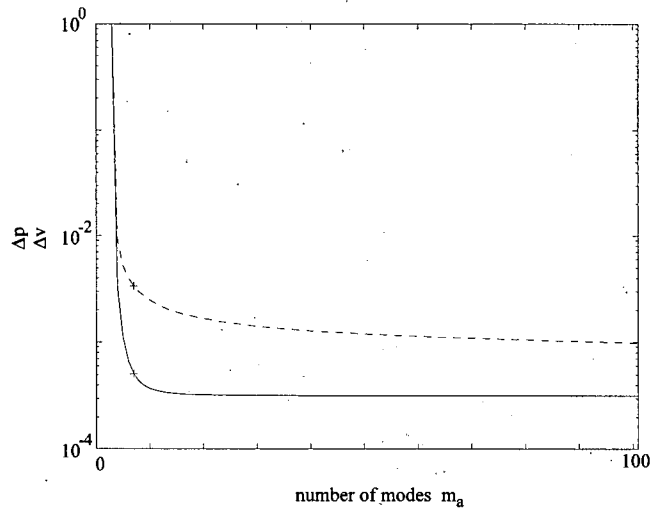


Fig. 2.11: pressure (solid) and velocity (dashed) convergence rates at 500 Hz

2.9.2 Coupled vibro-acoustic problem

2.9.2.1 Problem definition

A one-dimensional acoustic tube of length L_x is filled with a fluid with density ρ_0 and a speed of sound c . One end of the tube is rigid walled, while the other end consists of a piston with an infinitesimal area dy, dz and a mass per unit area m_s . The piston is elastically supported with a stiffness per unit area k_s and is excited by a dynamic force $F \cdot dy dz$ at frequency ω (see Fig. 1.12(a)).

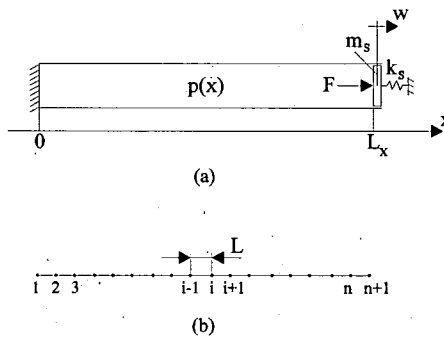


Fig. 2.12 : one-dimensional coupled problem (a) and its acoustic discretization (b)

The exact steady-state pressure response in the fluid and the exact steady-state piston displacement are

$$p_{exact}(x) = -\frac{\rho_0 c \omega F}{\rho_0 c \omega \cos\left(\frac{\omega L_x}{c}\right) + (k_s - m_s \omega^2) \sin\left(\frac{\omega L_x}{c}\right)} \cos\left(\frac{\omega x}{c}\right) \quad (2.130)$$

$$w_{exact} = \frac{F \sin\left(\frac{\omega L_x}{c}\right)}{\rho_0 c \omega \cos\left(\frac{\omega L_x}{c}\right) + (k_s - m_s \omega^2) \sin\left(\frac{\omega L_x}{c}\right)} \quad (2.131)$$

in which the harmonic time dependence $e^{j\omega t}$ is suppressed.

2.9.2.2 Model reduction techniques

As in the previous example, the steady-state pressure response in the fluid is approximated using a finite element discretization, which consists of n linear fluid elements with $(n+1)$ nodal pressure degrees of freedom (see Fig. 2.12(b)). The steady-state piston displacement is the single nodal degree of freedom of the structural FE model. The Eulerian FE/FE model (2.88) of the coupled vibro-acoustic system is

$$\begin{pmatrix} k_s & K_c \\ 0 & K_a \end{pmatrix} - \omega^2 \begin{pmatrix} m_s & 0 \\ -\rho_0 K_c^T & M_a \end{pmatrix} \cdot \begin{Bmatrix} w \\ p_1 \\ p_2 \\ \vdots \\ p_{n+1} \end{Bmatrix} = \begin{Bmatrix} F \\ 0 \\ 0 \\ \vdots \\ 0 \end{Bmatrix} \quad (2.132)$$

The $((n+1) \times (n+1))$ acoustic stiffness and mass matrices $[K_a]$ and $[M_a]$ are given in Eq. (2.122) and (2.123). The $(1 \times (n+1))$ coupling matrix $[K_c]$ is

$$[K_c] = [0 \ 0 \ \dots \ 0 \ -1] \quad (2.133)$$

The modal expansion technique, discussed in section 2.8.3.1, and the component mode synthesis technique, discussed in section 2.8.3.2, are applied to an Eulerian model (2.132) with $n=50$ fluid elements for the case of an air-filled ($\rho_0=1.225$ kg/m³, $c=340$ m/s) tube of length $L_x=1$ m with a piston ($m_s=1$ kg/m², $k_s=100000$ N/m³), excited by a force $F=1$ N/m² at frequency $\omega/2\pi=200$ Hz.

Fig. 2.13 compares the exact steady-state pressure and displacement with the corresponding prediction results, obtained with, on the one hand, an expansion with $m_c=5$ modes of the coupled system and, on the other hand, an expansion with the single structural degree of freedom and $m_a=4$ modes of the uncoupled acoustic system.

This figure clearly illustrates that, in comparison with a modal expansion model of the same size, the accuracy with a component mode synthesis model is significantly smaller, due to the zero fluid displacement in all uncoupled acoustic modes at the fluid-structure coupling interface ($x=1$).

As a result, the component mode synthesis technique requires a substantially larger modal base to get an accuracy, comparable with the accuracy of the modal expansion technique.

This is illustrated in Fig. 2.14, which plots the accuracy of the pressure and displacement predictions, indicated by their error measures Δp and Δv , defined in Eq. (2.124), against the number of modes in a modal expansion and a component mode synthesis model.

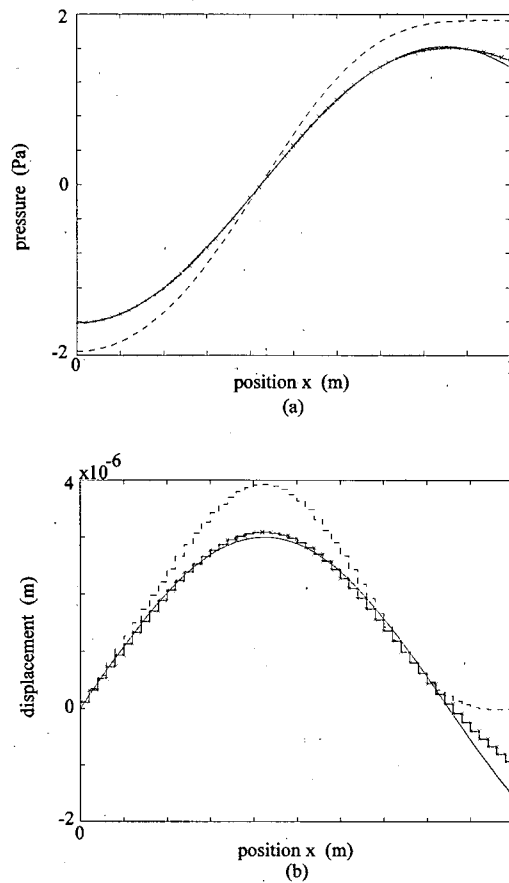


Fig. 2.13: instantaneous steady-state pressure (a) and displacement (b) at 200 Hz (solid: exact, x-marked: modal expansion ($m_c=5, n=50$), dashed : component mode synthesis ($m_a=4, n=50$))

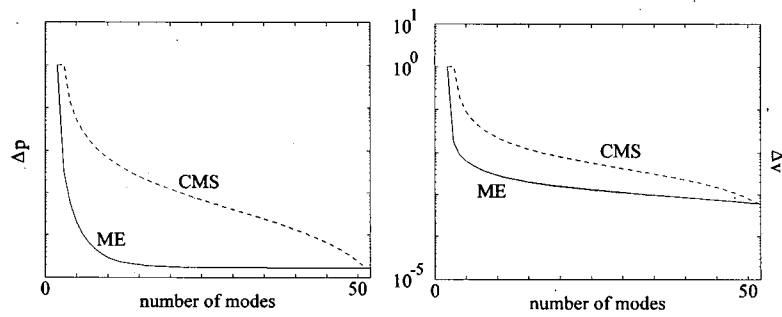


Fig. 2.14 : pressure (left) and displacement (right) convergence rates for modal expansion (solid) and component mode synthesis (dashed) models

2.10 References

- [2.1] Allik, H., Dees, R.N., and Moore, S.W., "Efficient structural acoustic analysis using finite and infinite elements", *Proceedings of the 1995 Design Engineering Technical Conferences* (Boston, 1995), Vol. 3 - part B ASME 1995, 87-95.
- [2.2] Assaad, J., Decarpigny, J.-N., Bruneel, C., Bossut, R., and Hamonic, B., "Application of the finite element method to two-dimensional radiation problems", *J. Acoust. Soc. Am.* **94**, 562-573 (1993).
- [2.3] Assaad, J., Bruneel, C., Rouvaen, J.-M., and Bossut, R., "An extrapolation method to compute far-field pressures from near-field pressures obtained by finite element method", *Proceedings of the 1995 Design Engineering Technical Conferences* (Boston, 1995), Vol. 3 - part B ASME 1995, 185-190.
- [2.4] Astley, R.J., "Wave envelope and infinite elements for acoustic radiation", *Int. J. Num. Meth. Fluids* **3**, 507-526 (1983).
- [2.5] Astley, R.J., and Eversman, W., "Wave envelope elements for acoustical radiation in inhomogeneous media", *Computers and Structures* **30**, 801-810 (1988).
- [2.6] Astley, R.J., Macaulay, G.J., and Coyette, J.P., "Mapped wave envelope elements for acoustical radiation and scattering", *J. Sound. Vib.* **170**, 97-118 (1994).
- [2.7] Astley, R.J., Macaulay, G.J., Coyette, J.P., and Cremers, L., "Three-dimensional wave-envelope elements of variable order for acoustic radiation and scattering. Part I: formulation in the frequency domain", *J. Acoust. Soc. Am.* **103**, 49-63 (1998).
- [2.8] Bathe, K.J., *Finite Element Procedures in Engineering Analysis* (Prentice Hall, Englewood Cliffs, New Jersey, 1982).
- [2.9] Bathe, K.J., Nitikitpaiboon, C., and Wang, X., "A mixed displacement-based finite element formulation for acoustic fluid-structure interaction", *Computers and Structures* **56**, 225-237 (1995).
- [2.10] Bayliss, A., and Turkel, E., "Radiation boundary conditions for wave-like equations", *Comm. Pure Appl. Math.* **33**, 707-725 (1980).
- [2.11] Bayliss, A., Gunzburger, M., and Turkel, E., "Boundary conditions for the numerical solution of elliptic equations in exterior regions", *SIAM J. Appl. Math.* **42**, 430-450 (1982).
- [2.12] Belytschko, T.B., "Fluid-structure interaction", *Computers and Structures* **12**, 459-469 (1980).
- [2.13] Bettess, P., *Infinite elements* (Penshaw Press, Sunderland, 1992).
- [2.14] Bettess, P., and Zienkiewicz, O.C., "Diffraction and refraction of surface waves using finite and infinite elements", *Int. J. Num. Meth. Eng.* **11**, 1271-1290 (1977).
- [2.15] Bossut, R., and Decarpigny, J.-N., "Finite element modeling of radiating structures using dipolar damping elements", *J. Acoust. Soc. Am.* **86**, 1234-1244 (1989).
- [2.16] Burnett, D.S., "A three dimensional acoustic infinite element based on a prolate spheroidal multipole expansion", *J. Acoust. Soc. Am.* **96**, 2798-2816 (1994).

- [2.17] Coyette, J.P., "Ritz vector synthesis versus modal synthesis for fluid-structure interaction modeling", *Proceedings of International Congress on Recent Developments in Air- and Structure-borne Sound and Vibration*, edited by Crocker, M.J. (Auburn, 1990), 115-126.
- [2.18] Coyette, J.P., "Validation of a new wave envelope formulation for handling exterior acoustic and elasto-acoustic problems in the frequency domain", *Proc. of the DGLR/AIAA 14th Aeroacoustics Conf.*, (Aachen, 1992), 421-427.
- [2.19] Coyette, J.P., and Dubois-Pélerin, Y., "An efficient coupling procedure for handling large size interior structural-acoustic problems", *Proceedings ISMA 19*, edited by Sas, P. (Leuven, 1994), 729-738.
- [2.20] Craggs, A., "The use of simple 3-D acoustic elements for determining natural frequencies of complex shaped cavities", *J. Sound Vib.*, **23**, 331-339 (1972).
- [2.21] Craggs, A., "An acoustic finite element approach for studying boundary flexibility and sound transmission between irregular enclosures", *J. Sound Vib.*, **30**, 343-347 (1973).
- [2.22] Craig Jr., R.R., "A review of time-domain and frequency-domain component-mode synthesis methods", *Int. J. Anal. & Exp. Modal Analysis* **2**, 59-72 (1987).
- [2.23] Craig Jr., R.R., and Bampton, M.C.C., "Coupling of substructures for dynamic analyses", *AIAA J.* **6**, 1313-1319 (1968).
- [2.24] Cremers, L., Fyfe, K.R., and Coyette, J.P., "A variable order infinite acoustic wave envelope element", *J. Sound. Vib.* **171**, 483-508 (1994).
- [2.25] Cura, F., Curti, G., and Scarpa, F., "State space methods in an Eulerian symmetrical formulation for vibroacoustics", *Modern Practice in Stress and Vibration Analysis*, edited by Gilchrist (Balkema, Rotterdam, 1997), 193-198.
- [2.26] Daniel, W.J.T., "Modal methods in finite element fluid-structure eigenvalue problems", *Int. J. Num. Meth. Eng.* **15**, 1161-1175 (1980).
- [2.27] Everstine, G.C., "A symmetric potential formulation for fluid-structure interactions", *J. Sound. Vib.* **79**, 157-160 (1981).
- [2.28] Feng, G.C., and Kiefling, L., "Fluid-structure finite element vibrational analysis", *AIAA J.* **14**, 199-203 (1976).
- [2.29] Givoli, D., Patlashenko, I., and Keller, J.B., "High-order boundary conditions and finite elements for infinite domains", *Comput. Methods Appl. Mech. Engrg* **143**, 13-39 (1997).
- [2.30] Gladwell, G.M.L., "A finite element method for acoustics", *Proc. of Fifth International Conference on Acoustics*, (Liège, 1965), paper L33.
- [2.31] Göransson, P., "On the representation of general damping properties in modal synthesis solutions of fluid structure interaction problems", *Proceedings of the DGLR/AIAA 14th Aeroacoustics Conference*, edited by DGLR, (Aachen, 1992), 679-686.
- [2.32] Hamdi, M.A., Ousset, Y., and Verchery, G., "A displacement method for the analysis of vibrations of coupled fluid-structure systems", *Int. J. Num. Meth. Eng.* **13**, 139-150 (1978).

- [2.33] Harari, I., and Blejer, G., "Finite element methods for the interaction of acoustic fluids with elastic solids", *Proceedings of the 1995 Design Engineering Technical Conferences* (Boston, 1995), Vol. 3 - part B ASME 1995, 39-48.
- [2.34] Heylen, W., Lammens, S., and Sas, P., *Modal Analysis Theory and Testing* (K.U.Leuven, 1995).
- [2.35] Hughes, T.J.R., *The Finite Element Method : Linear Static and Dynamic Finite Element Analysis* (Prentice Hall, Englewood Cliffs, New Jersey, 1987).
- [2.36] Ichikawa, T., and Hagiwara, I., "Coupled acoustic fluid-structure interaction analysis using component mode synthesis", *Proceedings InterNoise 94*, (Yokohama, 1994), 665-668.
- [2.37] Keller, J.B., and Givoli, D., "Exact non-reflecting boundary conditions", *J. Comput. Phys.* **82**, 172-192 (1989).
- [2.38] Luo, J., and Gea, H.C., "Modal sensitivity analysis of coupled acoustic-structural systems", *Journal of Vibration and Acoustics* **119**, 545-550 (1997).
- [2.39] Morand, H., and Ohayon, R., "Substructure variational analysis of the vibrations of coupled fluid-structure systems. Finite element results", *Int. J. Num. Meth. Eng.* **14**, 741-755 (1979).
- [2.40] Nefske, D., and Howell, L.J., "Automobile interior noise reduction using finite element methods", *Transaction SAE.*, **87**, 1727-1737 (1978).
- [2.41] Ohayon, R., "Variational analysis of a slender fluid-structure system: the elastic-acoustic beam", *Proceedings of NUMETA 85, Numerical methods in engineering: theory and applications*, edited by Middleton, J., and Pande, G.N. (Swansea, 1985).
- [2.42] Olson, L.G., and Bathe, K.J., "A study of displacement-based finite elements for calculating frequencies of fluid and fluid-structure systems", *Nucl. Eng. Design* **76**, 137-151 (1983).
- [2.43] Olson, L.G., and Bathe, K.J., "Analysis of fluid-structure interactions. A direct symmetric coupled formulation based on the fluid velocity potential", *Computers and Structures* **21**, 21-32 (1985).
- [2.44] Petyt M., Leas, J., and Koopman, G.H., "A finite element method for determining the acoustic modes of irregular cavities", *J. Sound Vib.*, **45**, 495-502 (1976).
- [2.45] Pinsky, P.M., Thompson, L.L., and Abboud, N.N., "Local higher-order radiation boundary conditions for the two-dimensional time-dependent structural acoustics problems", *J. Acoust. Soc. Am.* **91**, 1320-1335 (1992).
- [2.46] Sandberg, G., and Göransson, P., "A symmetric finite element formulation for acoustic fluid-structure interaction analysis", *J. Sound. Vib.* **123**, 507-515 (1988).
- [2.47] Szu, C., "Vibration analysis of structures using fixed-interface component modes", *Shock and Vibration Bull.* **46**, 239-251 (1976).
- [2.48] Thompson, L.L., "A multi-field space-time finite element method for structural acoustics", *Proceedings of the 1995 Design Engineering Technical Conferences* (Boston, 1995), Vol. 3 - part B ASME 1995, 49-64.
- [2.49] Thompson, L.L., and Pinsky, P.M., "A Galerkin least-squares finite element method for the two-dimensional Helmholtz equation", *Int. J. Num. Meth. Eng.* **38**, 371-397 (1995).

- [2.50] Wolf Jr., J.A., "Modal synthesis for combined structural-acoustic systems", *AIAA J.* **15**, 743-745 (1977).
- [2.51] Younes, T.A., and Hamdi, M.A., "Modal shapes reconstruction method for vibro-acoustic subdomains", *Proceedings of the 15th IMAC-Japan*, edited by Okubo, N. (Tokyo, 1997), 288-294.
- [2.52] Zienkiewicz, O.C., *The Finite Element Method - Vol. 1: Basic formulation and linear problems* (McGraw-Hill, London, 1977).
- [2.53] Zienkiewicz, O.C., and Bettess, P., "Fluid-structure dynamic interaction and wave forces. An introduction to numerical treatment", *Int. J. Num. Meth. Eng.* **13**, 1-16 (1978).
- [2.54] Zienkiewicz, O.C., and Taylor, R.L., *The Finite Element Method - Vol. 2: Solid and fluid mechanics, Dynamics and Non-linearity* (McGraw-Hill, London, 1991).

MFN 08-878

Enclosure 3

Affidavit

GE-Hitachi Nuclear Energy Americas LLC

AFFIDAVIT

I, **David H. Hinds**, state as follows:

- (1) I am the Manager, New Units Engineering, GE Hitachi Nuclear Energy ("GEH"), have been delegated the function of reviewing the information described in paragraph (2) which is sought to be withheld, and have been authorized to apply for its withholding.
- (2) The information sought to be withheld is contained in Enclosure 1 of GEH letter MFN 08-878, Mr. Richard E. Kingston to U.S. Nuclear Regulatory Commission, entitled *Response to Portion of NRC RAI Letter No. 220 Related to ESBWR Design Certification Application - DCD Tier 2 Section 3.9 – Mechanical Systems and Components; RAI Numbers 3.9-221, 3.9-222, 3.9-224, 3.9-225, 3.9-226, 3.9-227, 3.9-228, 3.9-229, 3.9-230, 3.9-231, & 3.9-232*, dated November 6, 2008. The GEH proprietary information in Enclosure 1, which is entitled *1. Response to Portion of NRC RAI Letter No. 220 Related to ESBWR Design Certification Application - DCD Tier 2 Section 3.9 – Mechanical Systems and Components; RAI Numbers 3.9-221, 3.9-222, 3.9-224, 3.9-225, 3.9-226, 3.9-227, 3.9-228, 3.9-229, 3.9-230, 3.9-231, & 3.9-232 - Proprietary Version*, is delineated by a [[dotted underline inside double square brackets.⁽³⁾]]. Figures and large equation objects are identified with double square brackets before and after the object. In each case, the superscript notation ⁽³⁾ refers to Paragraph (3) of this affidavit, which provides the basis for the proprietary determination. A non-proprietary version of this information is provided in Enclosure 2, *2. Response to Portion of NRC RAI Letter No. 220 Related to ESBWR Design Certification Application - DCD Tier 2 Section 3.9 – Mechanical Systems and Components; RAI Numbers 3.9-221, 3.9-222, 3.9-224, 3.9-225, 3.9-226, 3.9-227, 3.9-228, 3.9-229, 3.9-230, 3.9-231, & 3.9-232 - Public Version*.
- (3) In making this application for withholding of proprietary information of which it is the owner, GEH relies upon the exemption from disclosure set forth in the Freedom of Information Act ("FOIA"), 5 USC Sec. 552(b)(4), and the Trade Secrets Act, 18 USC Sec. 1905, and NRC regulations 10 CFR 9.17(a)(4), and 2.390(a)(4) for "trade secrets" (Exemption 4). The material for which exemption from disclosure is here sought also qualify under the narrower definition of "trade secret," within the meanings assigned to those terms for purposes of FOIA Exemption 4 in, respectively, Critical Mass Energy Project v. Nuclear Regulatory Commission, 975F2d871 (DC Cir. 1992), and Public Citizen Health Research Group v. FDA, 704F2d1280 (DC Cir. 1983).
- (4) Some examples of categories of information which fit into the definition of proprietary information are:
 - a. Information that discloses a process, method, or apparatus, including supporting data and analyses, where prevention of its use by GEH competitors without license from GEH constitutes a competitive economic advantage over other companies;

- b. Information which, if used by a competitor, would reduce his expenditure of resources or improve his competitive position in the design, manufacture, shipment, installation, assurance of quality, or licensing of a similar product;
- c. Information which reveals aspects of past, present, or future GEH customer-funded development plans and programs, resulting in potential products to GEH;
- d. Information which discloses patentable subject matter for which it may be desirable to obtain patent protection.

The information sought to be withheld is considered to be proprietary for the reasons set forth in paragraphs (4)a., and (4)b, above.

- (5) To address 10 CFR 2.390(b)(4), the information sought to be withheld is being submitted to NRC in confidence. The information is of a sort customarily held in confidence by GEH, and is in fact so held. The information sought to be withheld has, to the best of my knowledge and belief, consistently been held in confidence by GEH, no public disclosure has been made, and it is not available in public sources. All disclosures to third parties including any required transmittals to NRC, have been made, or must be made, pursuant to regulatory provisions or proprietary agreements which provide for maintenance of the information in confidence. Its initial designation as proprietary information, and the subsequent steps taken to prevent its unauthorized disclosure, are as set forth in paragraphs (6) and (7) following.
- (6) Initial approval of proprietary treatment of a document is made by the manager of the originating component, the person most likely to be acquainted with the value and sensitivity of the information in relation to industry knowledge, or subject to the terms under which it was licensed to GEH. Access to such documents within GEH is limited on a "need to know" basis.
- (7) The procedure for approval of external release of such a document typically requires review by the staff manager, project manager, principal scientist or other equivalent authority, by the manager of the cognizant marketing function (or his delegate), and by the Legal Operation, for technical content, competitive effect, and determination of the accuracy of the proprietary designation. Disclosures outside GEH are limited to regulatory bodies, customers, and potential customers, and their agents, suppliers, and licensees, and others with a legitimate need for the information, and then only in accordance with appropriate regulatory provisions or proprietary agreements.
- (8) The information identified in paragraph (2), above, is classified as proprietary because it identifies detailed GE ESBWR design information. GE utilized prior design information and experience from its fleet with significant resource allocation in developing the system over several years at a substantial cost.

The development of the evaluation process along with the interpretation and application of the analytical results is derived from the extensive experience database that constitutes a major GEH asset.

- (9) Public disclosure of the information sought to be withheld is likely to cause substantial harm to GEH's competitive position and foreclose or reduce the availability of profit-making opportunities. The information is part of GEH's comprehensive BWR safety and technology base, and its commercial value extends beyond the original development cost. The value of the technology base goes beyond the extensive physical database and analytical methodology and includes development of the expertise to determine and apply the appropriate evaluation process. In addition, the technology base includes the value derived from providing analyses done with NRC-approved methods.

The research, development, engineering, analytical and NRC review costs comprise a substantial investment of time and money by GEH.

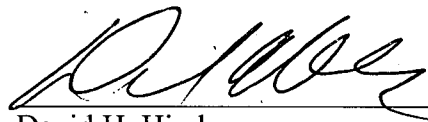
The precise value of the expertise to devise an evaluation process and apply the correct analytical methodology is difficult to quantify, but it clearly is substantial.

GEH's competitive advantage will be lost if its competitors are able to use the results of the GEH experience to normalize or verify their own process or if they are able to claim an equivalent understanding by demonstrating that they can arrive at the same or similar conclusions.

The value of this information to GEH would be lost if the information were disclosed to the public. Making such information available to competitors without their having been required to undertake a similar expenditure of resources would unfairly provide competitors with a windfall, and deprive GEH of the opportunity to exercise its competitive advantage to seek an adequate return on its large investment in developing these very valuable analytical tools.

I declare under penalty of perjury that the foregoing affidavit and the matters stated therein are true and correct to the best of my knowledge, information, and belief.

Executed on this 6th day of November 2008.



David H. Hinds
GE-Hitachi Nuclear Energy Americas LLC